UNIVERSITÀ DEGLI STUDI DI PADOVA

DIPARTIMENTO DI INGEGNERIA DELL'INFORMAZIONE

DIPARTIMENTO DI INGEGNERIA DELL'INFORMAZIONE

CORSO DI LAUREA IN ICT FOR INTERNET AND MULTIMEDIA - INGEGNERIA PER LE COMUNICAZIONI MULTIMEDIALI E INTERNET

"ANALYSIS OF ENVIRONMENTAL VIBRATIONS BASED ON OPTICAL FIBRE COMMUNICATION INFRASTRUCTURES"

Relatore: Prof. Luca Palmieri

Laureando: Nicolò Farella – Matr. 2026967

ANNO ACCADEMICO 2021-2022

Data di laurea 18/10/2022

CONTENTS

ACKNOWLEDGMENTS

ABSTRACT ITALIANO

Il seguente elaborato di tesi affronta l'argomento del rilevamento di eventi vibrazionali, quali movimenti sismici, con misure effettuate usando le infrastrutture di comunicazione in fibra ottica.

Il testo, dopo una sintetica esposizione in ordine alla situazione attuale delle odierne tecnologie di trasmissione coerente in fibra e il livello di sviluppo raggiunto nell'uso della fibra in applicazioni di sensoristica, illustra ed analizza le principali tecniche basate sulle fibre ottiche ad oggi usate per il rilevamento sismico.

Nella seconda parte dell'elaborato, mediante l'esame e la valutazione dei dati di equalizzazione di un canale in fibra, è esposta una dimostrazione del rilevamento degli eventi vibrazionali ottenuta applicando una delle tecniche precedentemente descritte.

ABSTRACT

The following thesis work addresses the topic of the detection of vibrational events, such as seismic movements, with measurements performed using fibre-optic communication infrastructures.

After a brief exposition on the current state of today's coherent fibre transmission technologies and the use of fibre in sensing applications, the text illustrates and analyses the main fibre-optic based techniques used for seismic sensing to date.

In the second part of the paper, by examining and evaluating the equalisation data of a fibre channel, a demonstration of the detection of vibrational events obtained by applying one of the previously described techniques is presented.

CHAPTER 1 — INTRODUCTION

Since the first experimental transmissions with optical fibre systems in 1977 [1] [2] the technologies employed have evolved to increase the capacity of the optical links; nowadays coherent optical transmission is the most widely used transmission method.

The first optical fibre communication systems of the 1970s employed intensity modulation of semiconductor lasers whose signal intensity was detected at the output by a photodiode, these systems where called *Intensity Modulated Direct Detection* (IMDD) systems; the receivers for IMDD systems are independent of the carrier phase and its state of polarization while coherent receivers, by interfering the input signal with a local oscillator (LO), are able to extract the phase information of a signal and are sensitive to the polarization of the signal.

Coherent receivers were studied since the 1980s but due to technical difficulties[1] and the success of erbium doped fibre amplifiers[2] in the 1990s they were shelved until 2008, the year of the commercialization of the first coherent optical communications system [3]. Digital coherent optical receivers enabled for adaptive electronic equalization of linear transmission impairments such as chromatic dispersion[3] and polarization mode dispersion[4], effects that were plaguing optical transmission systems in the early 2000s, and are relatively inexpensive to build in comparison with their analog electronic and optoelectronic counterparts [4].

Before the introduction of coherent transmission most systems used binary modulation formats such as on-off keying[5] or differential phase-shift keying[6] which encode only one bit per symbol; coherent communications on the other hand allows for digital access to the full optical field, increasing the spectral efficiency up to a factor of four [2] by encoding information onto other dimensions such as phase, frequency and polarization of the optical carrier granting the ability

---

[1] Coherent receivers at that time where costly and complex to build and presented problems related to phase-noise and polarization rotations.

[2] Erbium-doped fibre amplifiers (EDFA) can efficiently amplify light in the 1.5-μm wavelength region where the loss of telecom fibres are at a minimum; as a result of the usage of EDFAs a fibre optic link could support new modulation formats and higher bitrates.

[3] Chromatic dispersion is the phenomenon that causes different spectral components of a pulse to travel at different velocities, this is caused by the group velocity and the phase velocity of light propagating in the medium being dependant on the optical frequency.

[4] Polarization mode dispersion (PMD) is a form of dispersion where two different polarizations travelling along the fibre at the same speed, due to the asymmetries of the fibre, travel at different speeds.

[5] In on-off keying (OOK) data is encoded by sending a large amplitude carrier for encoding "1" and sending no carrier to encode "0".

[6] In differential phase-shift keying (DPSK) data is sent by changing the phase of the carrier wave.

to use both in-phase (I) and quadrature (Q) components and polarization-division multiplexing (PDM).

In the years after the introduction of coherent transmission new coding constellations were developed with rapidly growing symbol rates leading to an approximate rate increase of ~20%/year per laser carrier [2].

The operating principle of coherent receivers consists in mixing the received signal coherently with a continuous wave optical field before it passes through the photodetector, the optical signal from the transmitter is equal to

$$E_s(t) = A_s(t)\exp(j\omega_s t + \vartheta_s)$$

<div align="right">Eq. 1</div>

while the field of the local oscillator is

$$E_{LO}(t) = A_{LO}(t)\exp(j\omega_{LO} t + \vartheta_{LO})$$

<div align="right">Eq. 2</div>

Once mixed the resulting optical power incident on the photodetector is given by

$$P(t) = K|E_s(t) + E_{LO}(t)|^2$$

<div align="right">Eq. 3</div>

where K is a constant calculated as the ratio between the effective beam area and the impedance of free space. The previous equation can be rewritten as:

$$P(t) = P_s(t) + P_{LO} + 2\sqrt{P_s(t)P_{LO}}\cos(\omega_{IF} t + \vartheta_s - \vartheta_{LO})$$

<div align="right">Eq. 4</div>

where $\omega_{IF} = \omega_0 - \omega_{LO}$.

In the case where $\omega_{IF} = 0$ the resulting detector is called *Homodyne receiver*, in this type of receiver the input current from the homodyne receiver becomes

$$I(t) = 2R\sqrt{P_s(t)P_{LO}}\cos(\vartheta_s(t) - \vartheta_{LO}(t))$$

<div align="right">Eq. 5</div>

where R is the responsivity of the photodiode[7]. The use of homodyne detection allows to have an input power with an $4P_{LO}/P_s$ increase with respect to its direct detection counterpart leading to input power enhancements of up to 20dB and, as opposed to the direct-detection method, allows to transmit information via phase or frequency modulation.

---

[7] $R = q\eta/\hbar\omega_s$ where q is the electron charge, η the quantum efficiency of the photodiode and $\hbar$ is Plank's constant divided by 2π.

As it can be seen from the previous equation, the photodiode current only gives the cosine (in-phase) component of the signal while the quadrature component is lost so it is not possible to receive the full information of the signal complex amplitude with such system.

To detect both IQ components of the input light a second local oscillator, whose phase is shifted by $\pi/2$, is used; from this new configuration, called *phase-diversity homodyne receiver* or *intradyne receiver*, four outputs are obtained:

$$E_1 = \frac{1}{2}(E_s + E_{LO})$$
$$E_2 = \frac{1}{2}(E_s - E_{LO})$$
$$E_3 = \frac{1}{2}(E_s + jE_{LO})$$
$$E_4 = \frac{1}{2}(E_s - jE_{LO})$$
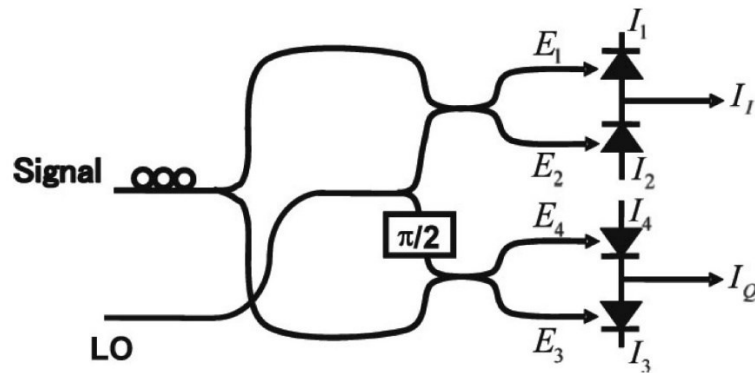
<div align="right">*Eq. 6*</div>

Figure 1 - System model of a phase-diversity homodyne receiver - Source: [5]

The photocurrents obtained by performing detection are then equal to:

$$I_I(t) = I_1(t) - I_2(t) = R\sqrt{P_s(t)P_{LO}}\cos(\vartheta_s(t) - \vartheta_{LO}(t))$$
$$I_Q(t) = I_3(t) - I_4(t) = R\sqrt{P_s(t)P_{LO}}\sin(\vartheta_s(t) - \vartheta_{LO}(t))$$

<div align="right">*Eq. 7*</div>

From the photocurrents obtained at the previous step it is then possible to recover the complex amplitude as

$$I_C(t) = I_I(t) + jI_Q(t)R\sqrt{P_s(t)P_{LO}}\exp\left(j(\vartheta_s(t) - \vartheta_n(t))\right)$$

<div align="right">*Eq. 8*</div>

where $\vartheta_n(t)$ is the total phase noise, calculated as $\vartheta_n(t) = \vartheta_{SHOT\ NOISE}(t) - \vartheta_{LO}(t)$.

By encoding two channels of information on two orthogonal polarization states it is possible to carry more information, to decode a polarization sensitive input the *polarization diversity*

receiver is used: this is composed by two phase-diversity homodyne receivers with two polarization beam splitters (PBS), one for the input signal and one for the local oscillator.
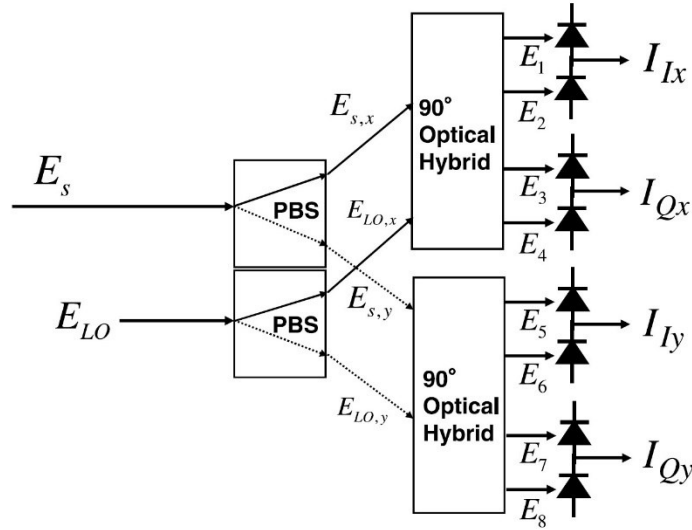

Figure 2 - Configuration of a polarization-diversity receiver - Source: [6]

In the case where, in equation 4, $|\omega_{IF}| \gg 2\pi/T$ the photocurrent becomes equal to

$$I(t) = R(P_s(t) + P_{LO}) + 2R\sqrt{P_s(t)P_{LO}}\cos(\omega_{IF}t + \vartheta_s - \vartheta_{LO})$$

Eq. 9

The first part of the previous equation can be considered as a constant since in these systems $P_{LO} \gg P_s$ and easily removed via band-pass filtering, thus the output photocurrent can be written as

$$I(t) = 2R\sqrt{P_s(t)P_{LO}}\cos\left(\omega_{IF}t + \vartheta_s(t) + \vartheta_n(t)\right)$$

Eq. 10

from which the complex amplitude of the input signal can be recovered

$$I_C = 2R\sqrt{P_s(t)P_{LO}}\exp\left(j\left(\vartheta_s(t) + \vartheta_n(t)\right)\right)$$

Eq. 11

The systems that make use of this type of detection are called *heterodyne receivers*, such systems have a lower SNR ratio improvement when compared to its homodyne counterpart[8] but offers a much more economic and simple configuration for the system.

Coherent detection thus allows the greatest flexibility in modulation formats as information can be encoded in multiple dimensions; coherent detection requires the receiver to have knowledge

---

[8]   The 3dB penalty is due to the signal power being the averaged value of $I^2(t)$ which contains a cosine (the average of $\cos^2$ is ½).

of the carrier phase as the received signal is demodulated by a local oscillator that serves as absolute phase reference.
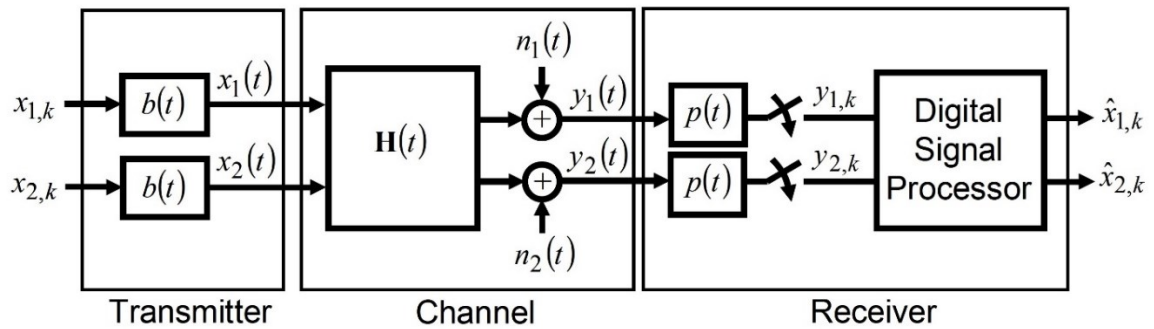

Figure 3 - System model of a coherent transmission system - Source: [4]

A coherent transmission system model is pictured above: in a typical system at the transmitter the TX laser output is split into its orthogonal polarization components before being modulated by two Mach-Zehnder modulators used to encode the symbols onto the carrier, once the modulation is complete the signals are recombined. After passing through the channel, which usually presents inline amplification, the signal arrives at the receiver where an optoelectronic downconverter recovers the baseband modulated signal with the techniques described above.

Despite being commonly known for their usage in long-haul communication infrastructures fibre optic cables are also widely employed in sensing and measurement: study for the usage of optical fibres for such applications began as early as 1960s (the Fiber Optic Proximity Probe was patented in the United States of America in 1967 [7]) and nowadays there are numerous realizations of fibre-optic sensors used to measure strain, temperature, pressure, current, voltage, gas, chemical contaminant, rotation, vibration, acceleration, bending, torsion, displacement and biomolecules [8]. In addition to the wide field of applications for fibre optic sensors the usage of such sensors also presents other advantages [9], the most important being:

- Increased sensitivity when compared to existing sensing techniques;
- Geometric versatility which allows configuration into arbitrary shapes;
- Immunity to radio frequency interference (RFI) and electromagnetic interference (EMI);
- High resistance to temperature, voltage and corrosive environments allowing the usage of such sensors in hostile media.

Fibre optic sensors also present an unique technique that is the ability to perform *distributed* measurements: in most sensing applications the parameter of interest is measured in a single

location but with fibre optics it is possible to use a long length of fibre as the sensing element[9] and thus allowing to make distributed measurements over distances up to several tens of kilometres [7] [10].

This thesis work is based on both of the fibre optic applications as the existing optical fibre network used for telecommunication can be repurposed as a distributed sensing device to perform environmental vibration monitoring. The thesis work will be structured as follows:

- A first chapter where fibre-based seismic sensing technologies will be discussed in detail and a comparison between them will be made.
- A second chapter detailing the analysis of the equalization data of an optical channel that will be used to study the environmental vibrations.
- Finally, a discussion of the results obtained by the analysis performed during the previous chapter.

---

[9]   It is also possible to have a fibre that is sensitive only along certain points, in this specific case the system is said to be *quasi-distributed*

CHAPTER 2 — FIBRE-BASED SEISMIC SENSING TECHNOLOGIES

Real-time monitoring of surface seismic activity around the globe is of great interest for a better understanding of Earth's internal structure but, as of today, most of the seismic stations sit on land; oceans and seas, despite covering 71%[10] of Earth's surface, remain mostly uncovered by seismic stations.
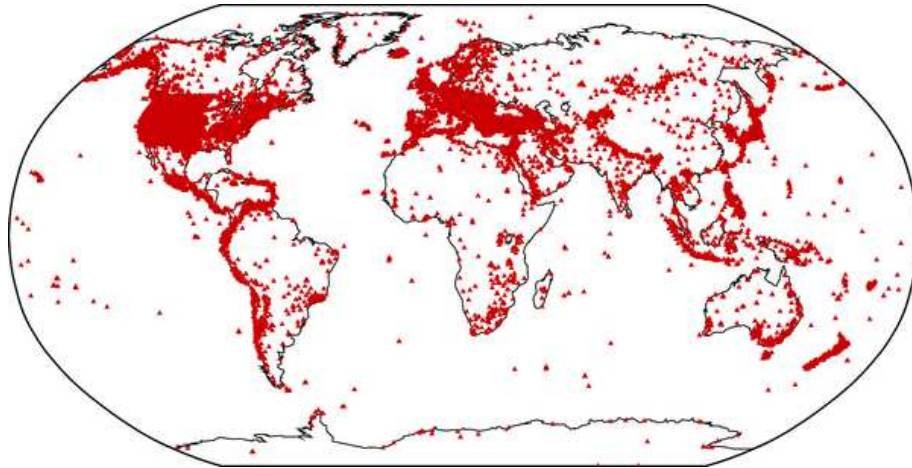

Figure 4 - Map of the seismic stations around the globe - Source: International Seismological Centre (ISC)

The already existing submarine telecommunication fibre-optic network, with its 1.3 million kilometres[11] widespread distribution, offers an ideal solution to this shortcoming of the seismic station network if used for distributed sensing.
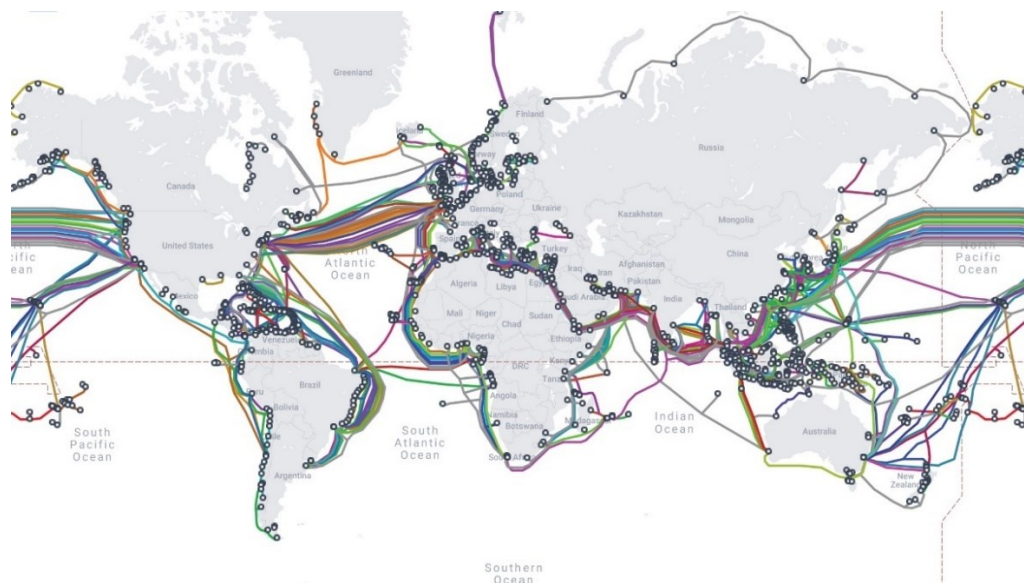

Figure 5 - Submarine Fibre-optic cable map - Source: TeleGeography

---

[10] Source: U.S. Geological Survey

[11] Source: TeleGeography

There are various types of optical seismic sensing technologies that can be used for this purpose: these are *Distributed Acoustic Sensing*, *Phase Monitoring* and *Polarization Monitoring*.

Distributed Acoustic Sensing

Distributed Acoustic Sensing (DAS) is a popular technique for geophysics applications, this is a type of distributed optical fibre sensor based on Rayleigh backscattering.

Rayleigh scattering is that effect for which light is elastically scattered by the small inhomogeneities[12] present in the fibre, a fraction of this scattered light is captured by the fibre core and guided back to the fibre input where its intensity can be measured [11] [12].

It is important to note that, as DAS makes use of backscattered light, the spatial range of such devices is limited to no more than 150km: DAS requires the transmission of high-power laser pulses to ensure high spatial resolution and a long enough reach [13] but the intensity of the received light rapidly decreases as only a portion of the scattered light is backscattered and the backscattered light intensity is inversely proportional to the fourth power of the intensity of the input beam.

By continuously pumping probe pulses in the fibre it is possible, thanks to the backscattered light, to build the backscattered trace of the fibre (the trace is unique to that specific tract), any perturbation in the surroundings of the fibre due to strain modifies its structure (either though a fibre elongation and/or a local change in the fibre refractive index) influencing the signature of that tract.
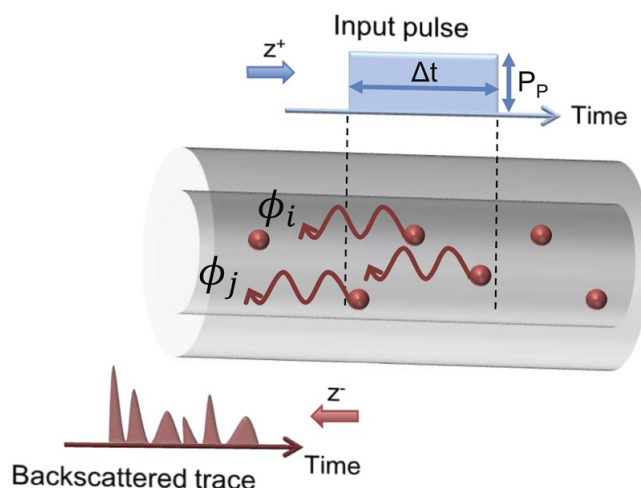

Figure 6 - Diagram of the operating principle of a DAS system - Source: [14]

---

[12]   The particles' radiuses are approximately less than about one-tenth the wavelength of the incident light in vacuum.

By calculating the time interval between the input probe-pulse and the received backscattered light it is possible to determine the exact location[13] where such perturbation has happened as

$$z = {c_0 t}/{2n}$$

where c_0 is the speed of light in vacuum, n the effective refractive index of the fibre and t the time since the probe-pulse was sent.

To estimate the magnitude of the external perturbations there are two possible techniques: by analysing the phase of Rayleigh backscattered light (OTDR approach) or by used a chirped probe pulse along with direct detection of the backscattered light intensity (OFDR approach).

Phase-demodulation-based DAS quantifies the perturbations by demodulating the optical phase of the trace: the phase accumulated over the propagation is equal to

$$\phi = 2zkn$$

where k is the wavenumber[14], n is the fibre effective refractive index and z is the length of the fibre through which light travels (multiplied by two to account for the roundtrip).

Any strain change causes a variation $\Delta\phi$ in the accumulated phase that can be written as:

$$\Delta\phi = \frac{4\pi}{\lambda_0}\Delta n \Delta z + \frac{4\pi}{\lambda_0} n\varepsilon\Delta z$$

where Δz is the perturbation length and ε is the strain[15] induced by the perturbation.

The effect of the perturbation can be seen as a variation of the effective refractive index:

$$\Delta n_{eff} = \Delta n + \varepsilon n$$

So equation 14 can be rewritten as:

$$\Delta\phi = \frac{4\pi}{\lambda_0}\Delta n_{eff}\Delta z$$

---

[13] Within the limits set by the spatial resolution of the probe-pulse and the accuracy of the estimation of the refractive index within that tract.

[14] $k = 2\pi/\lambda_0$

[15] $\varepsilon = \Delta d/\Delta z$

Temperature changes are also seen as variations of the effective refractive index so it is not possible to distinguish between a temperature or a strain perturbation but the ocean seafloor offers a stable temperature throughout the year so all the sudden external perturbations can be safely assumed to be due to strain.
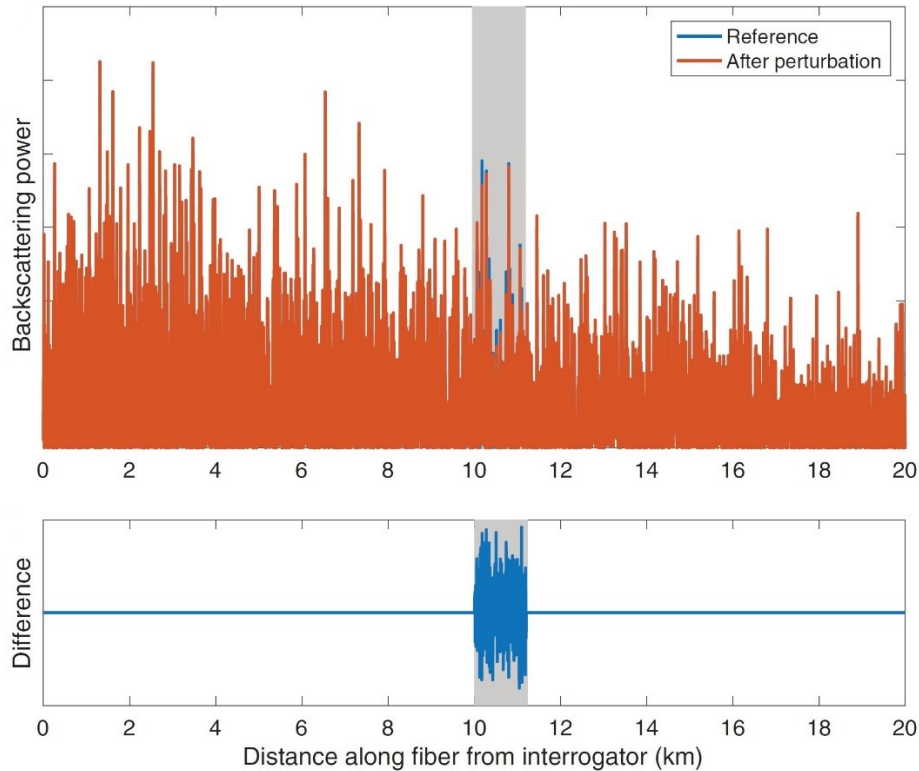

Figure 7 - Example of a detected perturbation on a backscattered trace - Source: [15]

Some problems arise from the need to use coherent detection [16]: the most detrimental problem to the use of DAS is the presence of *fading points*; fading points are some regions of the optical fibre where, due to Rayleigh backscattered light, no reliable measurement can be performed as the amplitude has such a low value that the phase reference is lost. This dependence on the amplitude also entails an uneven sensitivity of the DAS system. Fading points can be mitigated by using various strategies[16] and making an effective usage of post-processing interpolation algorithms.

The second approach to DAS is *chirped-pulse* DAS [17]; in this case the probe-pulse is linearly chirped and the received reflections are then mixed with a chirped reference and analysed within the frequency domain.

---

[16] For example using a Mach Zehnder modulator with a 3x3 coupler or using dual-probe pulses with different central frequencies.

The usage of probe-pulses whose signal has a sufficiently high chirp induces a frequency-to-time mapping of the trace, under a perturbation the bandwidth of the propagating probe-pulse experiences a shift within the perturbed region Δz proportional to the effective refractive index Δn_{eff}.
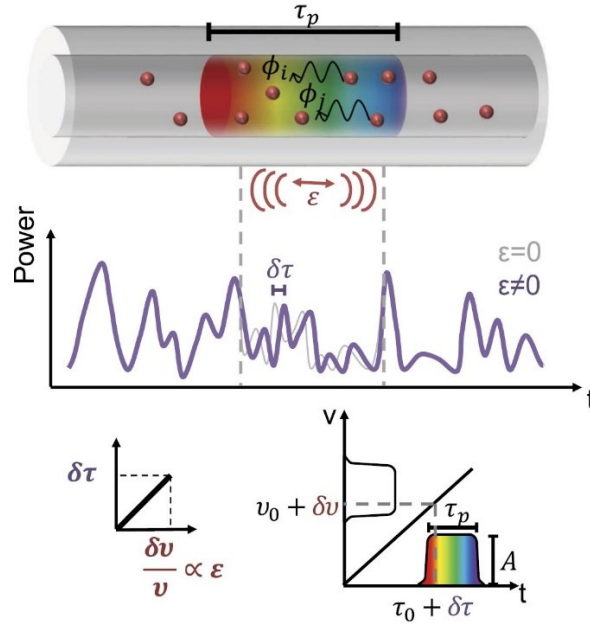

Figure 8 - Operating principle of a chirped-pulsed DAS - Source: [14]

To quantify the strength of the ongoing perturbation, a time delay estimation is made over the standard trace and the perturbed trace: the accumulated phase can be expressed as

$$\Delta\phi = \frac{4\pi}{\lambda_0}\frac{\Delta n_{eff}}{n}\frac{\Delta t}{2}c = 2\pi v_0 \frac{\Delta n_{eff}}{n}\Delta t$$

The frequency shift is then calculated as

$$\Delta v = \frac{1}{2\pi}\frac{d\Delta\phi}{d\Delta t} = v_0 \frac{\Delta n_{eff}}{n}$$

The temporal shift, proportional to the current perturbation, is then equal to

$$\delta t = v_0 \frac{\Delta n_{eff}}{n}\frac{\tau}{\delta v_p}$$

Chirped-pulse DAS, compared with Phase-demodulation-based DAS, does not require coherent detection, and thus neither sensitivity fading or polarization fading effects take place leading to a steady sensitivity that is not affected by intensity-fading of the detected trace [18]; despite this phase-demodulation-based DAS still remains the approach most used in most of the commercially available DAS [14].

Another drawback of both DAS types is that no communication other than the pulse-probe can be sent in the fibre thus requiring a fibre exclusively to perform DAS measurements: a solution to this problem can be found in the use of dark fibres, that are unlit fibres present in the submarine cables for backup, to carry on the pulse probe. This compromise however is not usable for every cable as some offer private networks on dark fibres. It is also important to note that, due to DAS range, it is not possible to cover the whole length of an oceanic cable without the use of proper distributed amplification or other pulse-modulation techniques[17] [14].

Among the many existing applications a fairly recent example of the application of DAS in seismology is an experiment conducted between 2017 and 2018 in Goldstone, California where dynamic strain rate measurements where performed on a 20 km fibre segment [19].
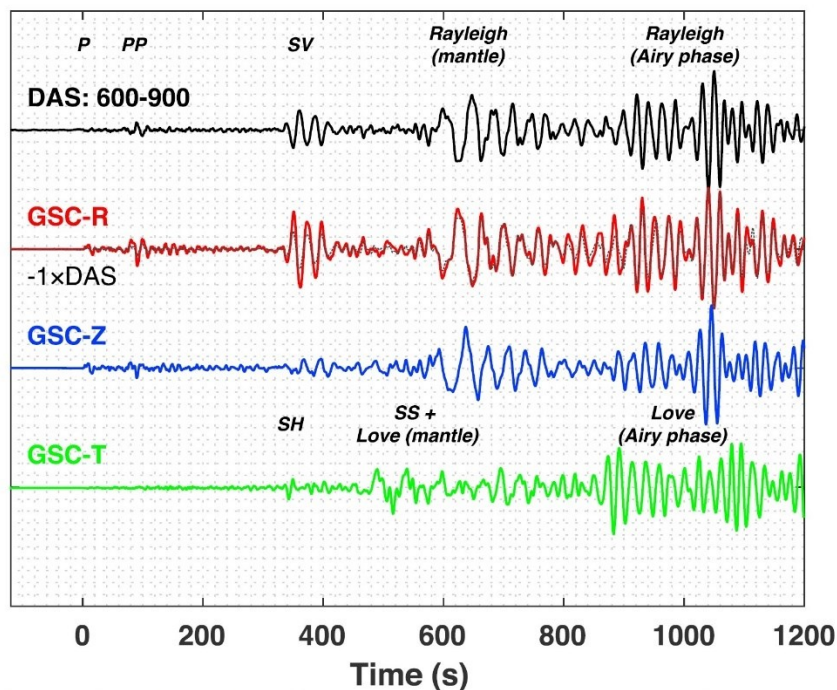

Figure 9 - Comparison between DAS strain and GSC particle velocity - Source: [19]

During the experiment various seismic events where detected, with the most noble being a 7.5 magnitude earthquake with epicentre in Honduras[18]; by comparing the stacked DAS strain waveforms from the channels whose orientations where almost parallel with the seism propagation direction and the data obtained from the broadband seismometer GSC installed a few kilometres away it can be seen that the results of the DAS are comparable with that of standard seismographic techniques.

---

[17]   The implementation of such techniques is feasible but costly and challenging.

[18]   Approximately 3807 km from the Goldstone Deep Space Communications Complex.

In comparison with classic seismic sensing techniques, the ability of the DAS system to perform distributed measurements allows to provide densely distributed travel time measurements to estimate of the epicentre of the received perturbation.

Phase Transmission fibre-optic sensing

A recent development in seismic sensing systems measures strain variations along the fibre by interferometric techniques [20] [21] and measuring the obtained signal at the end of the fibre or after a loop around it. These systems have a reach of hundreds or thousands of kilometres and can be used in conjunction with Wavelength Division Multiplexing (WDM) transmission as it only requires the allocation of a specific wavelength but, as the measurement is integrated and not distributed, the exact location of the perturbation along the fibre is not easily recovered. As in the case of DAS there are two main techniques that can be used to perform phase transmission sensing: the first consist in using microwave-range frequencies while the second method consists in using ultrastable laser interferometry.

In general, the time employed by a signal to reach location $\hat{x}(s) + d\hat{x}(s)$ from $\hat{x}(s)$[19] is equal to

$$dT = \frac{|d\hat{x}(s)|}{c[\hat{x}(s)]}$$

<div align="right">Eq. 20</div>

So the total travel-time along the fibre can be expressed as

$$T = \int_{s=0}^{L} \frac{ds}{c[\hat{x}(s)]}$$

<div align="right">Eq. 21</div>

When deformed a point $\hat{x}$ moves to $\hat{x} + \boldsymbol{u}(\hat{x}, t)$ where $\boldsymbol{u}(\hat{x}, t)$ is its displacement field so the total travel-time along the fibre can be rewritten as

$$T = \int_{s=0}^{L} \frac{|[\boldsymbol{I} + \boldsymbol{F}(\hat{x}, t)]\boldsymbol{e}(s)|}{c[\hat{x}(s), \boldsymbol{u}(\hat{x}, t)]} ds$$

<div align="right">Eq. 22</div>

where $\mathbf{F}$ is the deformation tensor defined as $\boldsymbol{F}(\hat{x}, t)d\hat{x} = \boldsymbol{u}(\hat{x} + d\hat{x}, t) - \boldsymbol{u}(\hat{x}, t)$ and $\mathbf{e}(\text{s})$ is the normalised tangent vector along the perturbed fibre.

---

[19] In this case $\hat{x}(s)$ is interpreted as a Lagrangian coordinate so its location moves with the deforming fibre instead of being fixed onto the reference frame.
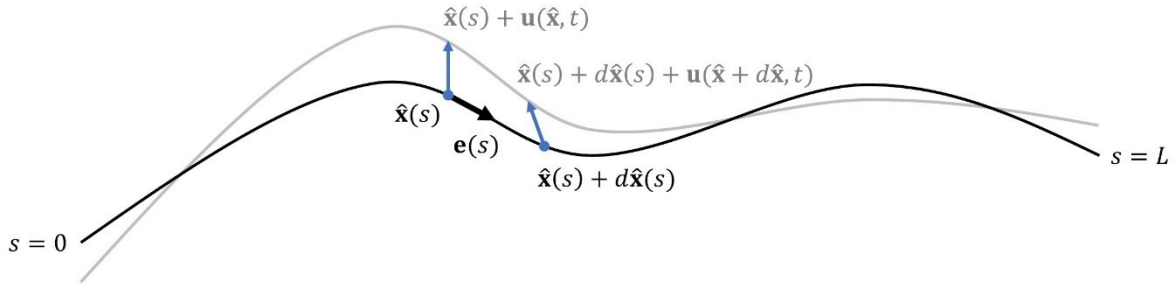
Figure 10 - Illustration of the fibre deformation - Source: [22]

In the case of a monochromatic input with frequency ω the phase difference is equal to

$$\phi(t) = \omega \Delta T(t) = \omega \int_{s=0}^{L} \frac{|[\boldsymbol{I} + \boldsymbol{F}(\hat{x}, t)]\boldsymbol{e}(s)|}{c[\hat{x}(s), \boldsymbol{u}(\hat{x}, t)]} ds - \omega \int_{s=0}^{L} \frac{ds}{c[\hat{x}(s)]}$$

Eq. 23

Since the displacement is usually in the micrometre range [23] equation n. 23 can be simplified to a first-order approximation

$$\delta_t \phi(t) \approx \frac{\omega}{c_0} \delta_t \int_{s=0}^{L} \tilde{n}[\hat{x}(s)] \varepsilon[\hat{x}(s), t] ds$$

Eq. 24

where $\tilde{n}$ is the sum of the refractive index of the fibre and the refractive index at rest caused by the perturbation along the fibre. A problem in the application of this method is that the fibre geometry should be known precisely as the deformation tensor $\boldsymbol{F}$ is influenced by it but fibre-optic cables can move during time giving rise to a number of false positives.

Even if the measurement is integrated it is possible to derive the point where the perturbation takes place along the fibre by transmitting the signal in both directions and then cross-correlating the signals received on both sides with their arrival time, by using two fibre cables in different position the epicentre of the perturbation can be found[20].

---

[20]   The precision of this method depends on the knowledge of the fibre route.
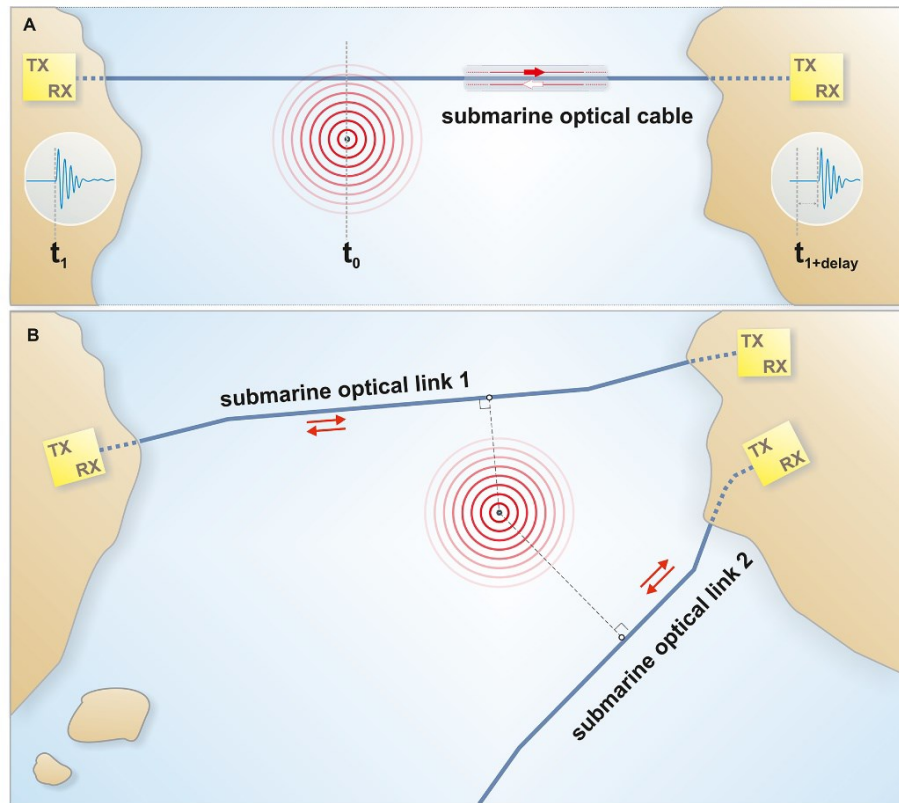
Figure 11 - Seismic event location technique - Source: [20]

As previously mentioned, there are two different techniques used to perform phase transmission sensing: the first consists in using microwave-range frequencies while the second method consists in using ultrastable laser interferometry.

The former sensing technique, called Microwave Frequency Fiber Interferometer (MFFI), was presented by Fichtner et al [22] [23] [24], this method consists in the dissemination of microwave carriers[21] superimposed on the optical wavelengths used for telecommunications and then performing interferometric measurements of the looped back microwave signal and a locally generated carrier providing the phase difference between the two; the phase difference then allows to estimate the strain and strain rate of the fibre.

In the experiment a 24 km fibre, located in Elefsina[22], Greece was used to perform both the aforementioned interferometric measurement and DAS measurements[23]; during the experiment several seisms where detected with the most notable being a 6.3 magnitude earthquake near Crete, approximately 380 km from the input end of the fibre.

---

[21] For the experiment frequencies above 10 GHz where used.

[22] Also known as Eleusis.

[23] The amplitude of the average DAS signal is smaller than any of the individual channels as the averaging leads to interference.
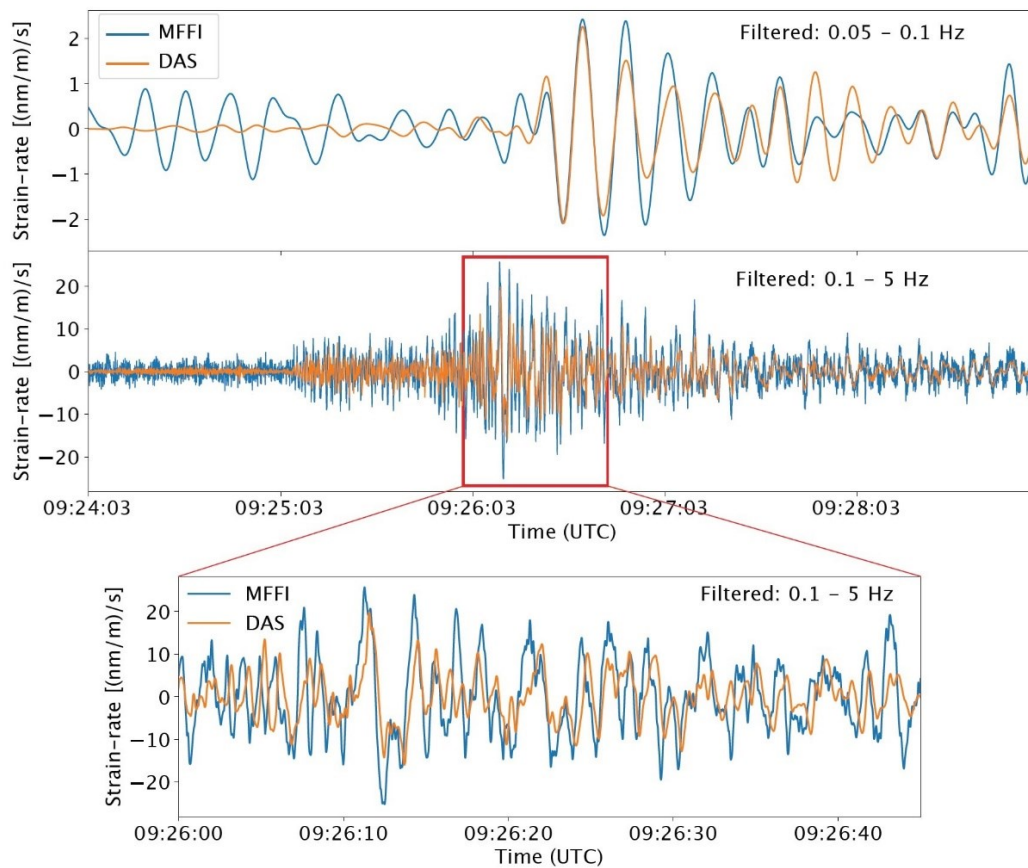
Figure 12 - Comparison between the MFFI output and the DAS averaged signals in the time domain – Source: [23]

The strain rates of the two systems are comparable to each other in both time and frequency domain.
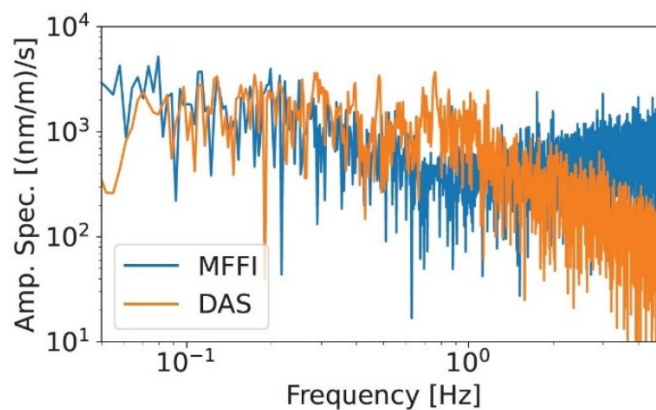

Figure 13 - Comparison between the MFFI output and the DAS averaged signals in the frequency domain – Source: [23]

By being an integrated system measurements performed with MFFI do not provide any indication of the position of the seism epicentre; additionally the MFFI sensitivity is highly dependent on the curvature of the employed fibre so the geometry of the chosen fibre should be known beforehand as small events on straight sections could not be perceived leaving gaps in the system.

The second method used to perform phase transmission sensing relies on the use of ultra-stable laser interferometry [20]: the system operates similarly to the previous one but offers a much higher sensitivity due to the use of a coherent source[24]. With the use of this techniques various earthquakes were detected with the most notable being a magnitude 7.5 earthquake on the Iraq-Iran border that was detected by a fibre in Italy, 3100 km from the epicentre, and a fibre in England, 4100 km from the epicentre.
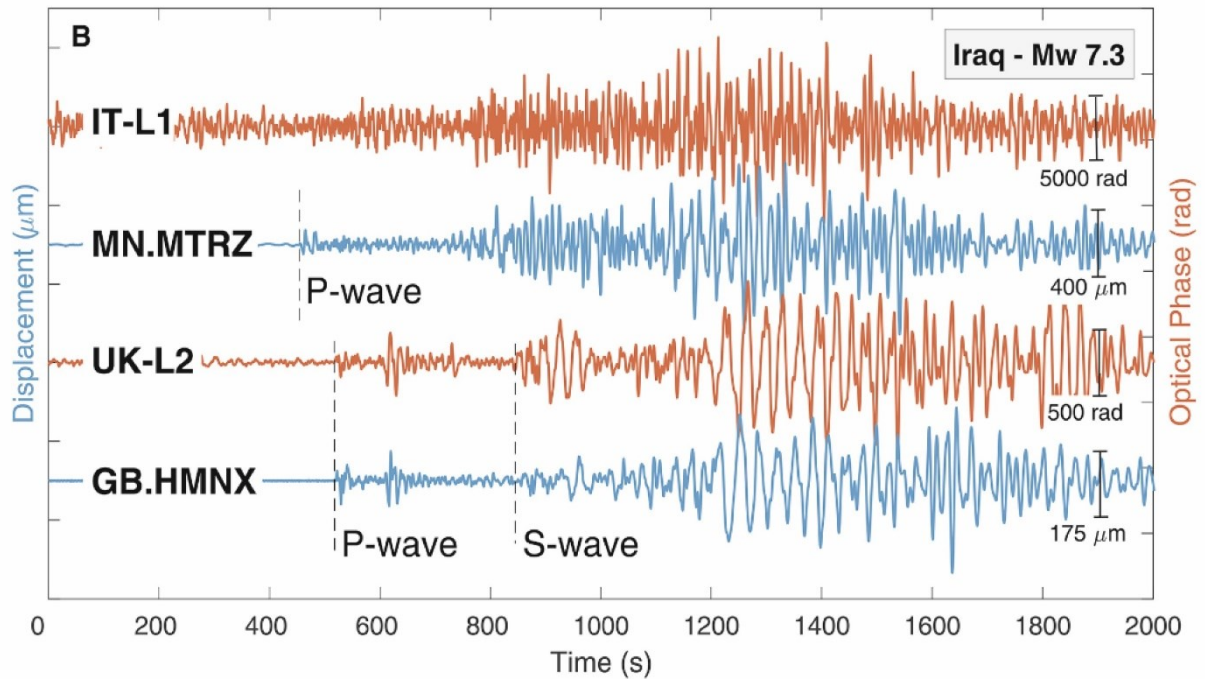

Figure 14 - Comparison between the interferometric measurements and the signal from a seismometer - Source: [20]

By comparing the phase changes on the links (IT-L1 and UK-L2) with the signals from seismometers located near the two links[25] it is possible to see that the results of this method are comparable with those obtained with a standard seismographic measurement.

The sensitivity of the system depends on the location of the fibre itself: the links considered in the example are both terrestrial fibre links and both are influenced by man-made noise, this effect is particularly evident on the Italian fibre where the P-wave could not be perceived due to the noise. The same measurement, performed using submarine links, has a noise floor from 5 to 8 times lower than that of a terrestrial fibre and thus submarine links allow for the detection of low magnitude vibrational events.

---

[24] Thus also resulting more expensive to implement.

[25] Monterenzio (MN.MTRZ) seismometer for Italy and Herstmonceux (GB.SWN1) seismometer for Britain.

Optical polarization−based seismic sensing

In polarization-based sensing the seismic activity is detected by the changes over the state of polarization, this is a parameter used for channel estimation for digital signal processing and so it does not require, unlike the previous method, the transmission of additional signals along the fibre; as for phase transmission sensing the measurement is integrated over the whole fibre so the exact position of the perturbation cannot be easily located.

For its correct operation coherent polarization multiplexing systems require the knowledge of the input/output polarization relationship, these are known in the form of Jones Matrices. Considering a light beam propagating in the z direction the beam can be described by

$$\boldsymbol{E}(\boldsymbol{r},t) = \boldsymbol{A}\cos{(\omega t - \boldsymbol{k}\boldsymbol{r})}$$

<div align="right"><i>Eq. 25</i></div>

This beam can be broken down into two mutually independent components[26] as

$$\begin{cases} E_x(t) = A_x\cos{(\omega t + \delta_x)} \\ E_y(t) = A_y\cos{(\omega t + \delta_y)} \end{cases}$$

<div align="right"><i>Eq. 26</i></div>

These two components can be expressed in exponential format as

$$\begin{cases} E_x(t) = A_x e^{j(\omega t + \delta_x)} = A_x e^{j\omega t} e^{j\delta_x} \\ E_y(t) = A_y e^{j(\omega t + \delta_y)} = A_y e^{j\omega t} e^{j\delta_y} \end{cases}$$

<div align="right"><i>Eq. 27</i></div>

where $A_x e^{j\delta_x}$ and $A_y e^{j\delta_y}$ are the complex amplitudes with which the polarization state of the beam can be completely described, the *Jones Vector* is then the complex amplitudes of the beam expressed as a column vector

$$\bar{a} = \begin{bmatrix} a_x \\ a_y \end{bmatrix} = \begin{bmatrix} A_x e^{j\delta_x} \\ A_y e^{j\delta_y} \end{bmatrix}$$

<div align="right"><i>Eq. 28</i></div>

If the previously described light beam passes through a polarising element the output beam is equal to

$$a'_x = J_{xx}a_x + J_{xy}a_y$$
$$a'_y = J_{yx}a_x + J_{yy}a_y$$

<div align="right"><i>Eq. 29</i></div>

---

[26] Considering the time evolution at the origin z=0.

where $J_{xx}, J_{xy}, J_{yy}, J_{yx}$, are the transforming factors of the polarising element (in this case the optical fibre) and are the elements that constitute the *Jones Matrix*.

$$J = \begin{bmatrix} J_{xx} & J_{xy} \\ J_{yx} & J_{yy} \end{bmatrix}$$

So with the knowledge of the Jones Matrix of the fibre it is possible to perform virtual interferometric measurements [25] reproducing the injection of a wave with a fixed polarization and examining the obtained polarization at the end of the link.

As briefly mentioned before in an ideal single-mode fibre there is not a single mode propagating through it but rather two degenerate orthogonal polarization modes; any construction flaw or external stress breaks the perfect symmetry of the fibre and causes the two degenerate modes to become uncoupled.

External stress applied to the fibre cause the fibre structure to become birefringent: birefringence is that effect for which the silica structure of the fibre becomes more ordered and thus causing the passing light to see a different value of the dielectric permeability depending on the polarization orientation with respect to the stress direction.

The complex amplitudes at the output of a fibre with constant birefringence are equal to

$$\begin{cases} a_x(z) = a_x(0)e^{-j\beta_x z} \\ a_y(z) = a_y(0)e^{-j\beta_y z} \end{cases}$$

where β_x and β_y are the two propagations constants. Recalling equation 27 and 28 these can be also expressed in vector form as

$$\bar{a}(z) = \begin{pmatrix} a_x(z) \\ a_y(z) \end{pmatrix} = \begin{pmatrix} e^{-j\beta_x z} & 0 \\ 0 & e^{-j\beta_y z} \end{pmatrix} \begin{pmatrix} a_x(0) \\ a_y(0) \end{pmatrix} = J(z)\bar{a}(0)$$

Birefringence strength is characterized by the *polarization beat length L_B* that is given by

$$L_B = \frac{2\pi}{\Delta\beta}$$

where $\Delta\beta$ is the difference between β_x and β_y.

The birefringence is obviously not uniform along the fibre so the whole fibre has to be considered as a concatenations of pieces of fibres with beat lengths in the order of metres with different orientations and birefringence.

The light polarization can be expressed in a more convenient wave in the form of *Stokes Vectors* [26].

Given the Jones vector defined in equation 28 the corresponding Stokes vector is defined as:

$$\bar{S} = \begin{pmatrix} S_0 \\ S_1 \\ S_2 \\ S_3 \end{pmatrix} = \begin{pmatrix} |a_x|^2 + |a_y|^2 \\ |a_x|^2 - |a_y|^2 \\ 2Re[a_x a_y^*] \\ 2Im[a_x a_y^*] \end{pmatrix}$$

<div align="right">Eq. 34</div>

These can be rewritten in the form of *unit Stokes Vectors*, that are given by dividing the last three Stokes parameters by S_0, that is the total beam intensity.

$$\hat{s} = \begin{pmatrix} s_1 \\ s_2 \\ s_3 \end{pmatrix} = \frac{1}{|a_x|^2 + |a_y|^2} \begin{pmatrix} |a_x|^2 - |a_y|^2 \\ 2Re[a_x a_y^*] \\ 2Im[a_x a_y^*] \end{pmatrix}$$

<div align="right">Eq. 35</div>

The unit Stokes vector cover a unit sphere called *Poincaré sphere*; the evolution of the unit Stokes vector $\hat{s}$ on a section of fibre with constant birefringence β is represented on the Poincaré spere as a rotation around the vector $\vec{\beta}$.

$$\frac{d\hat{s}}{dz} = [\vec{\beta}(z)] \times \hat{s}$$

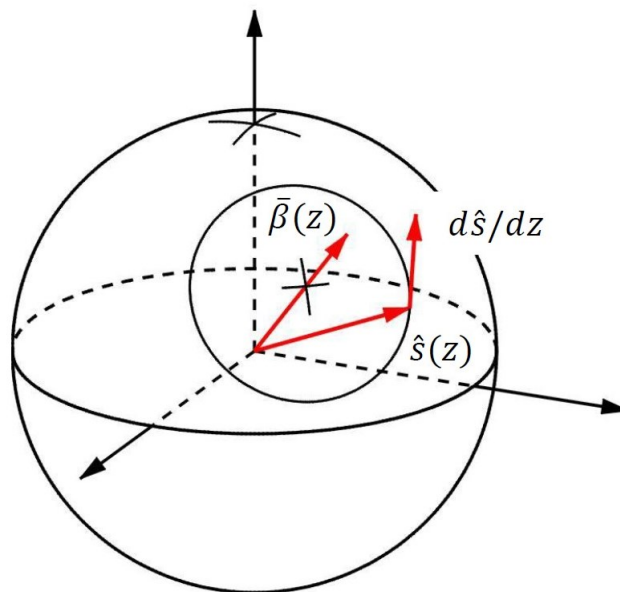<div align="right">Eq. 36</div>

Figure 15 - Evolution of the unit Stokes vector on the Poincaré sphere - Source: Fiber Optics course slides, 2021

If the fibre is affected by time-dependent external perturbation the trajectory along the Poincaré sphere is no longer circular and can be expressed as:

$$\frac{d\hat{s}}{dz} = [\vec{\beta}(z) + \Delta\vec{\beta}(z,t')] \times \hat{s}$$

<div align="right">Eq. 37</div>

with $t' = t - nz/c_0$ but in the case of fast perturbations $t \sim t'$ as for seismic application the slow drift that characteries standard telecommunication fibres can be safely ignored.

The evolution of the unit Stokes vector along the fibre is the concatenation of different rotations around $\Delta\vec{\beta}'(z,t)2L_F$ where $\Delta\vec{\beta}'(z,t)$ is the perturbation birefringence rotated back[27] by the static birefringence $\vec{\beta}(z)$ from z to the input [27] and where L_F is the birefringence correlation length, that is the length over which the birefringence decorrelates.

If the variation of the unit Stokes vector $|\Delta\hat{s}| \ll 1$ the following holds true:

$$\Delta\hat{s}(t) \cong \sum_{i=1}^{N} \Delta\vec{\beta}'(z_i,t)2L_F \times \hat{s}(0)$$

<div align="right">Eq. 38</div>

so the deviation of the unit stokes vector is the sum of randomly oriented vectors whose magnitude is proportional to the birefringence perturbation in that segment.

From the above equations, it is possible to derive [25] an equation linking the measured change of the unit Stokes vector to the strength of the perturbation as

$$\langle\Delta\hat{s}^2\rangle = \frac{\pi}{4}\left(\frac{2\pi c}{\lambda}\right)^2 \int_0^z k^2 \frac{\langle\Delta\vec{\beta}^2\rangle}{\langle\vec{\beta}^2\rangle} dz'$$

<div align="right">Eq. 39</div>

This equation shows that for a given birefringence perturbation the polarization modulation at the output is proportional to the local PMD of the fibre and thus allowing the fibre to be used for distributed sensing using this technique.

A real fibre cable is both affected by slow perturbations and fast perturbations: the slow perturbations cause a long-term drift of the polarization that is detrimental to the study of the fast perturbations of interest. To remove the slow perturbations effect on the Stokes vectors a moving window average is performed with a certain time window *t* and then renormalised to unit length to have the averaged Stokes vectors sit on the surface of the Poincaré sphere; after this step a rotation is applied to the Stokes vectors in such a way that the moving average is always centred on an arbitrary reference point of the Poincaré sphere. By following this

---

[27] Removing the birefringence rotation has no effect on the calculations as the relative orientation between vectors remains preserved.

procedure the Stokes vector values that diverge from the chosen reference point are the perturbations faster than the time window *t*.

This technique was recently applied in an experiment [28] on the Curie cable, a 10429 km long submarine fibre optic cable that connects Los Angeles (USA) with Valparaiso (Chile). During the test period various seims where captured with the most relevant being a magnitude 7.4 earthquake with epicentre in Oaxaca, Mexico, approximately 500 km from the cable.
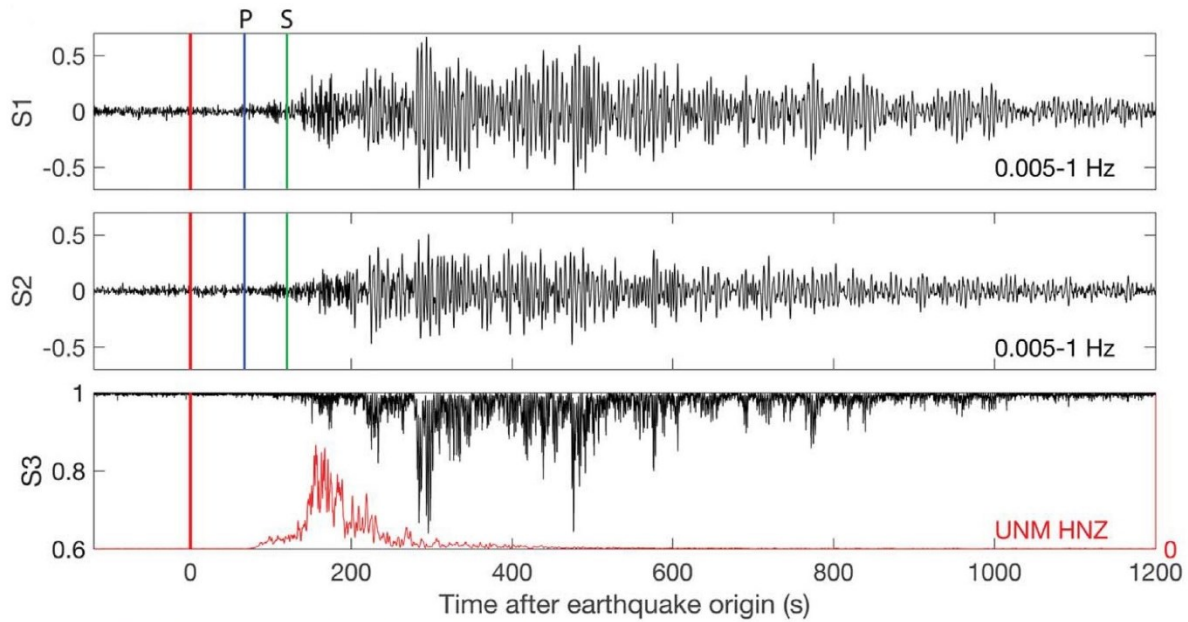

Figure 16 - Perturbations of the Stokes vectors compared with a seismograph measurement - Source: [28]

Due to the integrated measurement of polarization sensing and the considerable length of the fibre, as it can be seen on the graph above, the very start of the perturbation is not accurately detected and the signal has and has a long tail, exceeding the real end of the perturbation.

Comparison between techniques

Among the previously described seismic sensing techniques only DAS is widely used in commercial applications (the first DAS system was patented in 1993[28]) while the other sensing techniques have only recently (2018 for phase transmission fibre-optic sensing and 2021 for optical polarization–based seismic sensing) been studied so at the time of writing no commercial applications for both phase transmission fibre-optic sensing and optical polarization–based seismic sensing exist.

---

[28]   United States Patent: 5194847 - Apparatus and method for fiber optic intrusion sensing

There is no doubt that over the years phase and polarization seismic sensing will be employed for seismic sensing but DAS will continue to be used for sensing over relatively small areas (nowadays DAS are widely used for distributed strain measurements in the gas and oil industry).

Comparing the three techniques to each other DAS has the advantage of having a relatively high sensitivity [13] and has the capacity to perform precise localization of the perturbation; DAS however has a short range and requires costly equipment in the form of a DAS interrogator and a dedicated fibre to perform measurements. Phase seismic sensing on the other hand has a sensitivity comparable with that of DAS but with a reach of even tens of times that of a DAS system, however it does not allow for easy localization of the perturbation and requires the use of the techniques described above, effectively requiring a synchronized system on the other end of the fibre or the use of a second fibre. Phase seismic sensing does not require a dedicated fibre but it can lean on the existing fibre infrastructure by using a fraction of the transmitted spectrum to send the needed signal.

Polarization seismic sensing as phase seismic sensing performs an integrated measurement over the fibre and has a similar maximum reach but it does not need dedicated hardware and does not need the allocation of a portion of the optical bandwidth as its measurements are based on the set of parameters used for channel estimation for coherent transmission, this advantage however comes at the price of a lower sensitivity both when compared to phase seismic sensing and DAS.

CHAPTER 3 — CASE STUDY

In this thesis work equalization data from an optical channel will be analysed to perform polarization seismic sensing with the techniques described in the previous chapter.

Experimental Setup

The data under study is provided by the *Innovating City Planning Through Information and Communications Technologies* (INCIPIT) project of the University of L'Aquila; the aim of the INCIPIT project is to create an experimental optical network to build a Metropolitan Area Network (MAN) for the city of L'Aquila.

Figure 17 - Satellite map of the INCIPIT Project - Source: incipict.univaq.it

The INCIPIT Infrastructure is comprised of two optical rings: the longer ring, of about 20km in length, uses multi-mode fibres while the shorter ring, of about 6km in length, comprises three different types of multi-core fibres among which there is the fibre cable used to obtain the data that will be analysed further into this chapter.

Multi-core fibres are employed for space-division multiplexing (SDM): space-division multiplexing refers to that multiplexing technique whereby cables containing multiple cores or spatial modes are used as parallel channels for independent signals; multi-core fibres thus share a single common cladding for the many cores contained within.

Multi-core fibres can be broadly divided into two categories: uncoupled MCF[29] (UC-MCF), where the crosstalk is limited due to the distance separation between the various cores, and

---

[29]   Sometimes also called weakly-coupled MCF.

Strongly-Coupled MCF that can, in turn, be divided into Randomly-Coupled MCF (RC-MCF) and Systematically-Coupled MCF.

Randomly coupled MCF present a strong random-mode mixing between the modes, thanks to this it can achieve an higher spatial density compared to uncoupled MCF and the random-mode coupling provides a natural suppression for the accumulation of nonlinear interference noise and other mode-dependent impairments [29]; this advantages comes at the cost of requiring a multiple-input-multiple-output (MIMO) digital signal processing (DSP) to compensate for the random coupling while UC-MCF does not require any specific equipment compared to standard single-mode fibres.

Systematically-coupled MCF have the strongest coupled cores of all the different typologies of MCF, in the case of such strong coupling the multiple cores act as a single multimode waveguide system so along the fibre cable there is the propagation of a *supermode[30]*. This type of cable offers a very high transmission rate but requires a complex system for multiplexing and demultiplexing [30].

The INCIPIT Project within the smaller fibre ring holds a jelly-filled 6.29 km MCF cable of 6mm of outer diameter that contains 18 fibre strands [31]: twelve of them are randomly coupled four-core MCF (RC-4CF), two are uncoupled eight-core MCF (UC-8CF) and the remaining four are uncoupled four-core MCF (UC-4CF) from which the data to be analysed is sourced from.
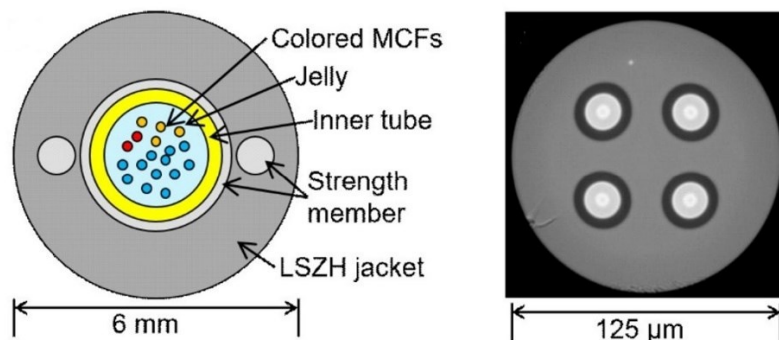

Figure 18 - Schematic of the cross section of the MCF cable (left) and cross-section photograph of an UC-4CF strand (right) - Source: [31]

The four strands of UC-4CF are concatenated with each other, the output is then connected to a fan-out and then back to a fan-in to go through the system twice for a total path length of 50.32km. The Jones Matrix of the system is measured at a clock rate of 125MHz with a decimation factor of 65536 that leads to a resolution of about 524μs (1907Hz). The used DSP

---

[30] A coupled mode can be seen as the superposition of the various isolated modes, hence the name.

is running using a non-phase sensitive equalizer leaving the phase handling to a separate DSP stage.

Data Analysis

The analysed data, gathered between February 9 and February 11 2022, is divided into files, each comprised of 13633536 Jones Matrices (1.985 hours per file) totalling to 36 files for a little less than three full days of measurement data.

Before calculating any parameter the raw input data is analysed by itself: by a cursory look of the elements comprising the Jones matrices it can be seen that the input data is sometimes subject to an erroneous correction by the DSP that results in the rotation of the Jones matrix elements around the origin of the complex plane.

To address this problem the following procedure is used: the mean position of the elements of the Jones Matrices on the first file that does not present such behaviour is calculated (in this case the chosen file is the third one), the coordinate of this point is used to find the angle between the reference "block" and the blocks to rotate back into position.
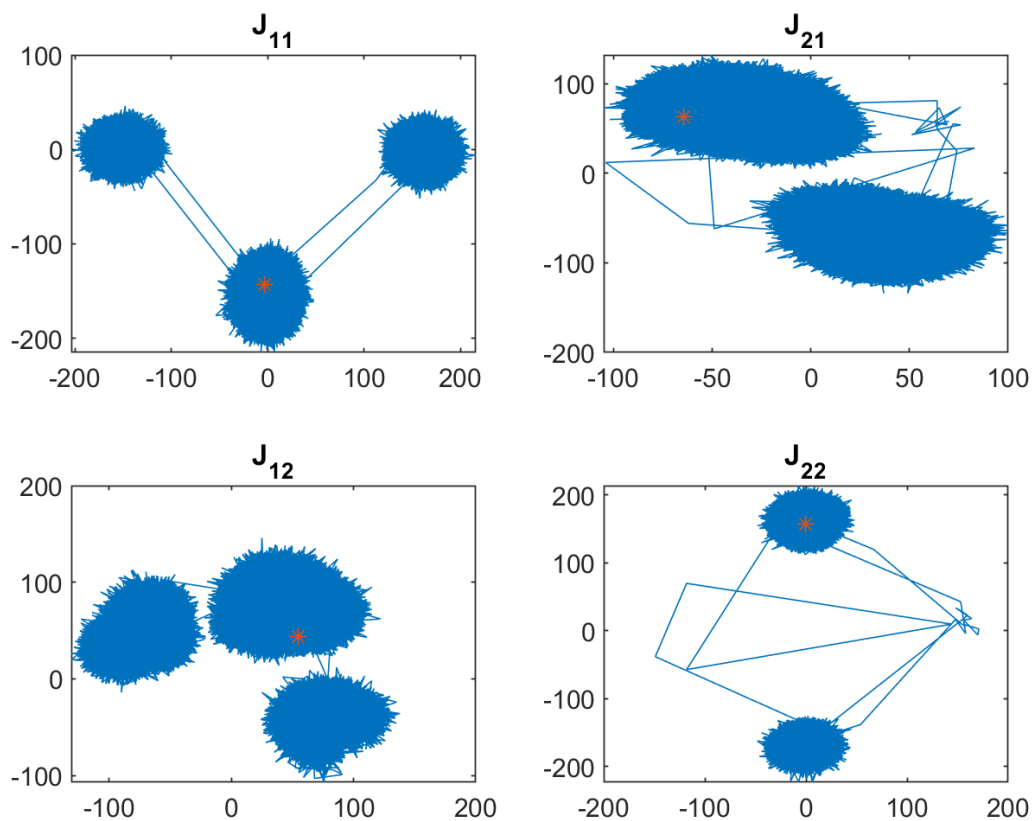
Figure 19 - Example of a portion of a portion of raw Jones matrices: the red asterisk marks the mean position of the reference block

With such angle calculated then the blocks are rotated back in place by multiplying their Jones matrices by the desired angle as

$$J_{Corrected} = \begin{bmatrix} J_{xx}e^{-j\varphi_{correctionxx}} & J_{xy}e^{-j\varphi_{correctionxy}} \\ J_{yx}e^{-j\varphi_{correctionyx}} & J_{yy}e^{-j\varphi_{correctionyy}} \end{bmatrix}$$

<div align="right">Eq. 40</div>

where $\varphi_{correction}$ are the desired angles used for the rotation. In the case of this thesis work only angles multiple of $\pi/4$ are used thus sometimes leaving some "smudges" on the corrected data which, however, can be easily discerned from other real phenomena as they appear on the various calculated parameters as sudden peaks. With the input data corrected it is now possible to proceed with the actual data analysis.

As described in the previous chapter with the knowledge of the Jones Matrix of the fibre it is possible to perform virtual interferometric measurements [25] and examining the obtained polarization at the end of the link. To perform such operation the injection of a wave with a fixed polarization is performed, in this case both an horizontally linearly polarized and a vertically linearly polarized inputs are used[31]; the output Jones vector obtained by using this procedure are then converted into Stokes vectors by using equation 34.

For plotting such a large amount of data the calculated values are first smoothed with the use of a Lowess filter[32] and then resampled at 10 Hz; both the filtering and the resampling will be removed further into the analysis when the elaborated data has to be closely examined to look for external perturbations.

The first of the four elements comprising the Stokes vector, S_0, is the signal intensity, that is plotted below:
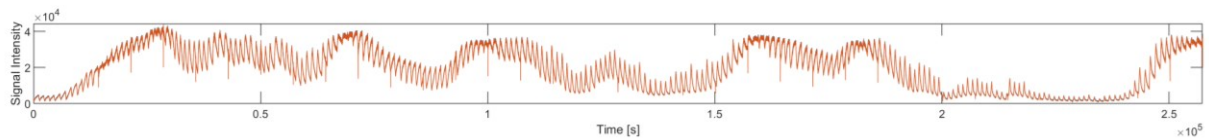

<div align="center">Figure 20 - Signal intensity evolution of the recorded data</div>

By examining the graph it is possible to see that there are two distinct moments where the signal intensity value is extremely low, these areas are the very start of the recording, so when the system was first turned on and towards the end of the recording for unknown reasons. The other parameters calculated from the data pertaining to these two sectors undergoes heavy fluctuations and cannot be considered reliable so for the purpose of this analysis all the data belonging to those areas is ignored in the following sections.

---

[31]   All the following plots are for a linear horizontal polarization unless stated otherwise.

[32]   Local regression using weighted linear least squares and a 1st degree polynomial model.

After removing such files, the degree of polarization is calculated starting from the Stokes vectors: the degree of polarization, as the name suggests, is the portion of the output light that is polarised. Such value is calculated as:

$$\mathcal{P} = \frac{I_{pol}}{I_{tot}} = \frac{\sqrt{S_1{}^2 + S_2{}^2 + S_3{}^2}}{S_0}$$
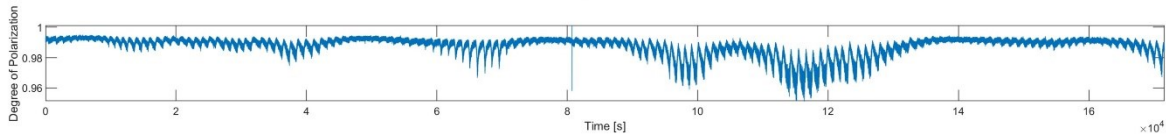
with $0 \leq \mathcal{P} \leq 1$.

Figure 21 - Evolution of the degree of polarization of the recorded data

As it can be seen from the above graph the degree of the polarization of the output is very high as expected since the input is fully polarized.

By dividing the last three Stokes parameters by S_0 the Stokes vectors are converted into unit Stokes vectors that can be plotted onto the Poincaré sphere.
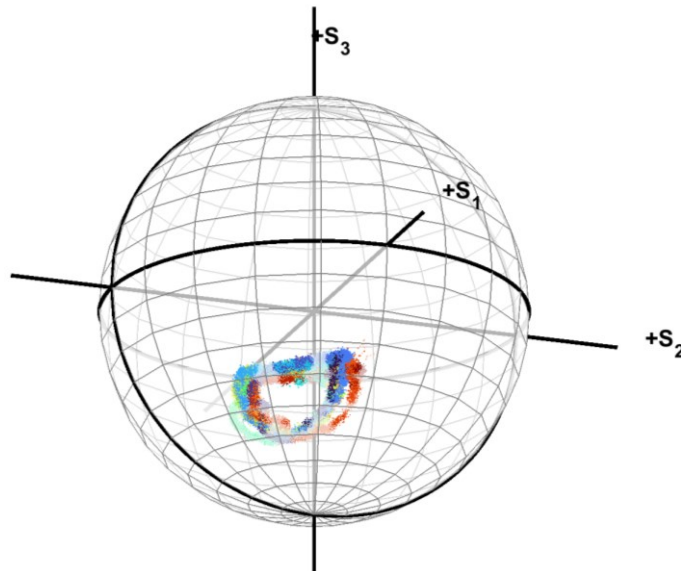

Figure 22 - Evolution of the SOP for a portion of the data

From figure 22, that represents the evolution of the state of polarization of the output light for a single file, it can be seen that the evolution of the SOP follows the expected behaviour: it draws circles around the rotation vector ϕ while said vector moves along the Poincaré sphere.
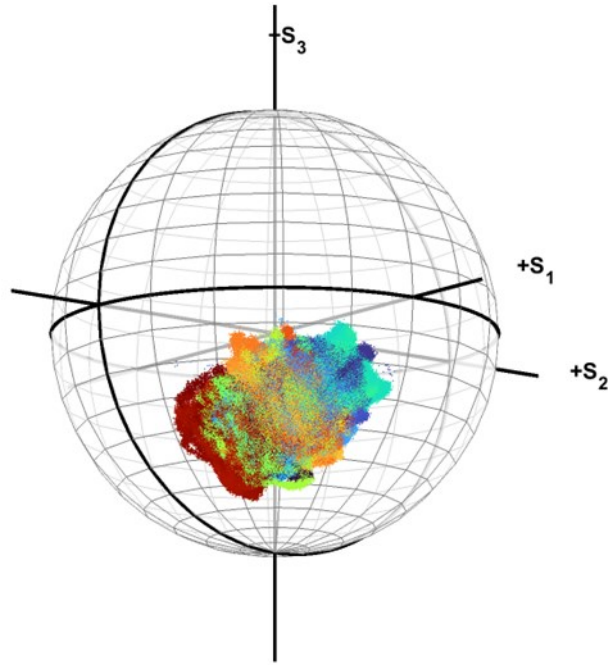
Figure 23 - overall evolution of the SOP along the Poincaré sphere

The evolution of the state of polarization is affected by both slow and fast perturbation but, for the purposes of this analysis, the interest lies into the fast perturbation such as earthquakes. To remove the effect of slow perturbations on the unit Stokes vectors the unit Stokes vectors are rotated by a certain angle in such a way that the average unit Stokes vector over a moving window of 100s always sits on a reference vector $\widehat{S_m}$ on the Poincaré sphere (in this case chosen to be the horizontal linear polarization[33]).

The rotation matrix to apply to the stokes vectors is calculated as:

$$R(\vartheta, \hat{v}) = I + sin\vartheta(\hat{v} \times) + (1 - cos\vartheta)(\hat{v} \times)^2$$

where ϑ is the angle between the average unit Stokes vector and the reference vector and $\hat{v}$ is a vector found by

$$\hat{v} = \frac{\widehat{S_m} \times \widehat{S_1}}{\left\|\widehat{S_m} \times \widehat{S_1}\right\|}$$

By multiplying the rotation matrix found with this procedure with the unit Stokes vectors the new unit Stokes vectors centred on the reference vector.

---

[33]   Whose corresponding unit Stokes vector is $s_1 = [1 \quad 0 \quad 0]$.
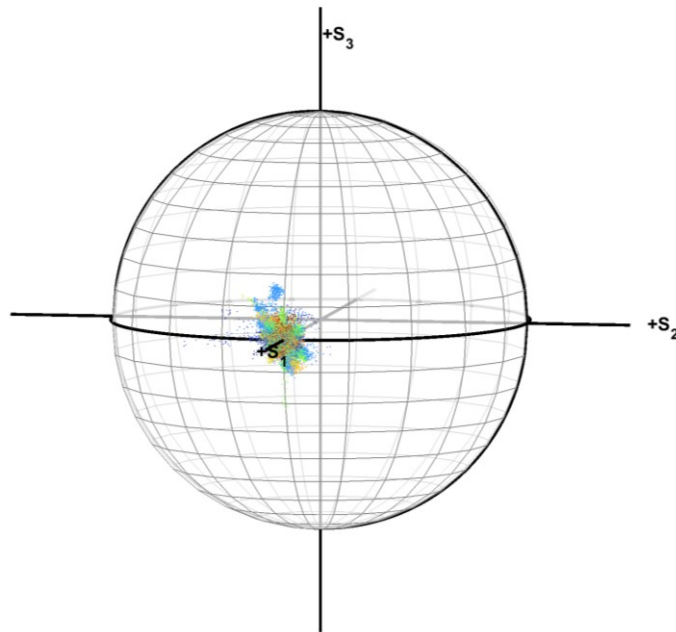
Figure 24 - overall evolution of the stabilised SOP

The unit Stokes vectors plotted on the Poincaré sphere above that do not sit onto the reference vector s_1 are those points that undergo perturbations faster than 100s. It is important to note that those points do not represent for the most part the external perturbations but they are effects of the periodicity of the signal. To better study this effect the spectra for the stabilized Stokes vectors is computed.
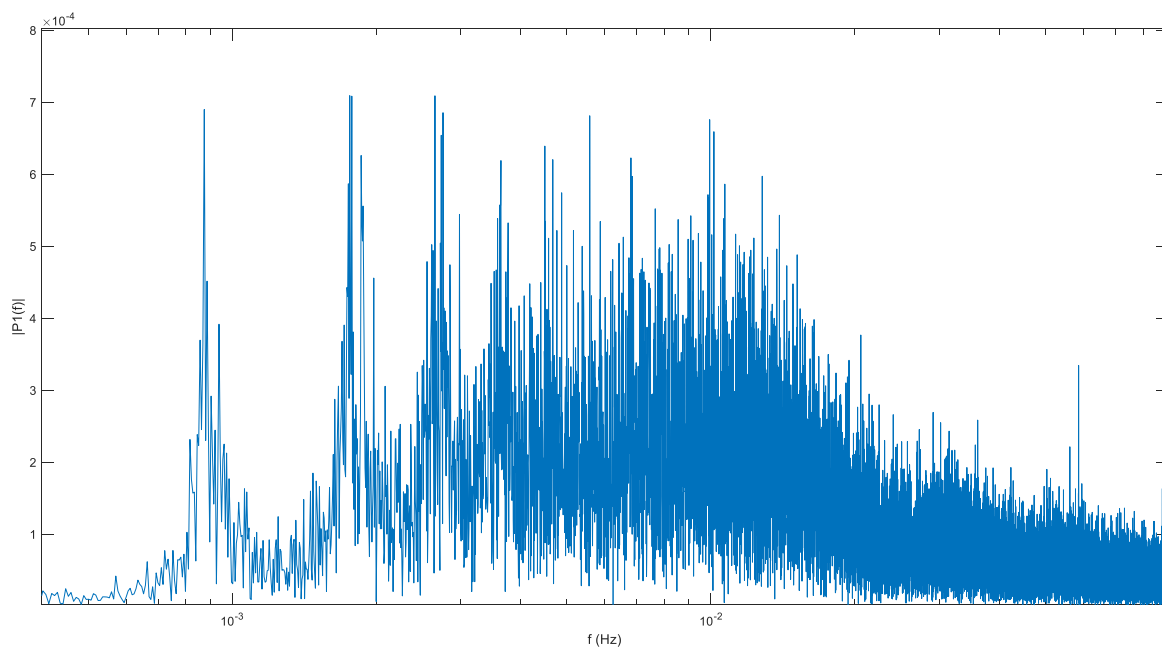

Figure 25 - Spectrum in the low frequency range for the stabilized values of s_2

Regarding the low frequency components plotted in the above spectrum there are three noticeable peaks on the leftmost side: these are the peaks with frequency of 0.0008742Hz (~19 min), 0.001760Hz (~9.47 min) and 0.002652Hz (~6.28min). These peaks, especially the first

one, is clearly visible from the previous plots of the total beam intensity (figure 20) and the degree of polarization (figure 21).

To visualise the higher frequencies the Lowess filtering is removed as it also acted as a low pass filter.
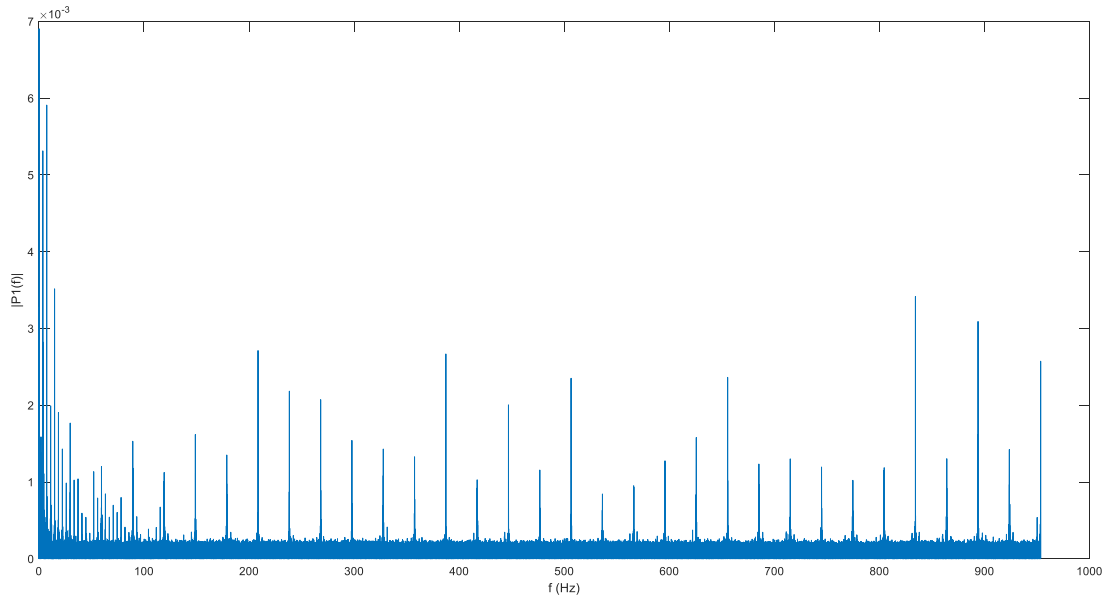

Figure 26 - full spectrum for the stabilized values of s_2

From the analysis of the spectrum three frequencies stand out: 0.1173Hz (~8.52s) and then 3.72Hz whose relevant harmonics can be seen up until ~125Hz and 29.79Hz, an harmonic of 3.72Hz, whose harmonics can be seen on the whole spectrum.
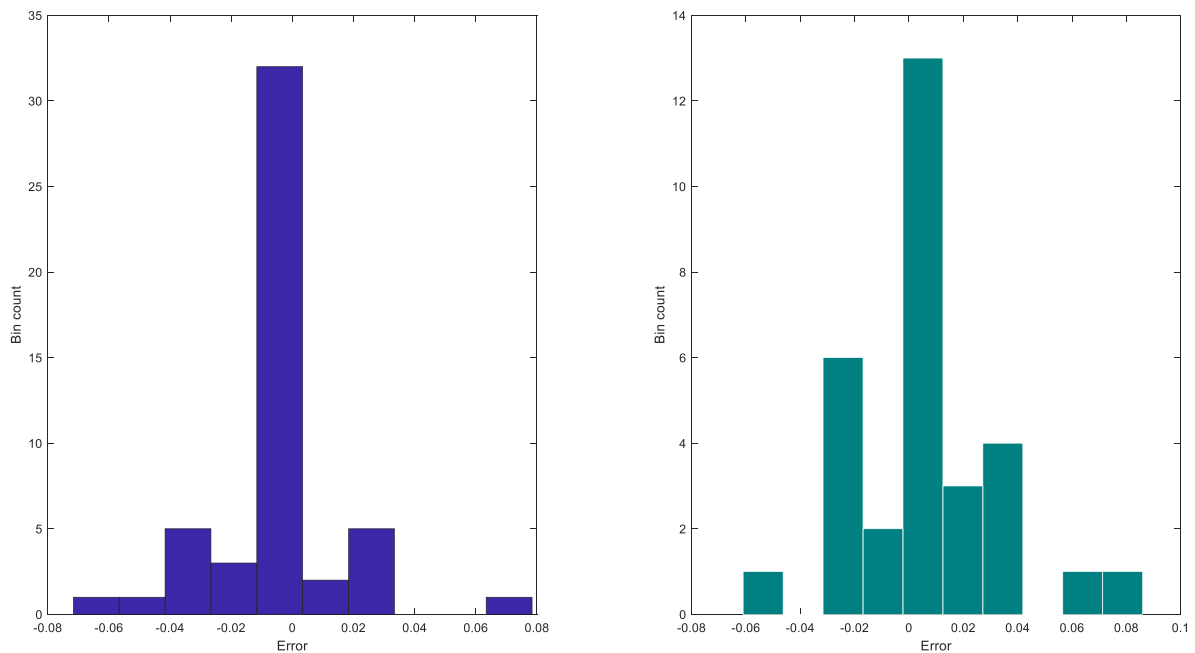

Figure 27 - Error distribution for harmonics of 3.72Hz (left) and for harmonics of 29.79Hz (right)

These frequency values can be easily seen onto a spectrogram as in figure 28.
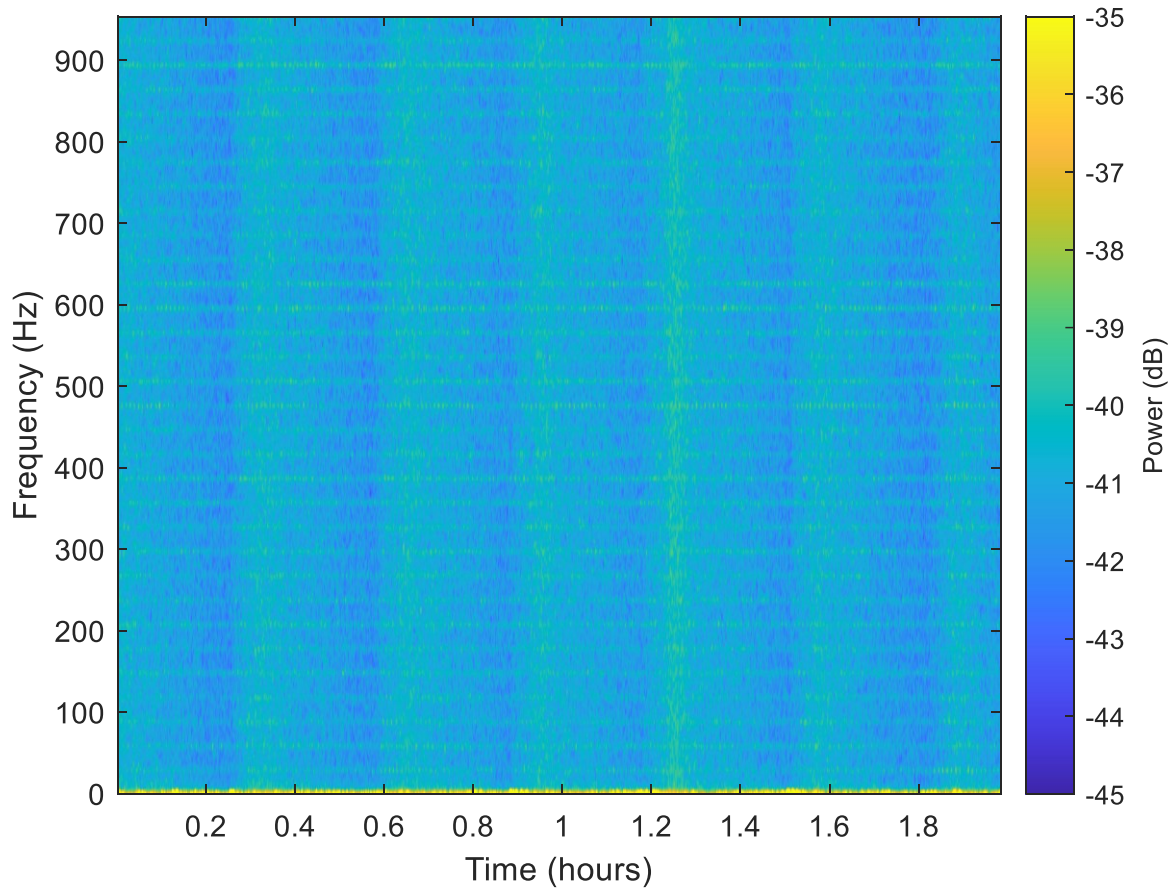
Figure 28 - Spectrogram for a portion of the data

To better understand the evolution of the output signal the rotation vector is calculated: this value is estimated starting from the unitary part of the Jones Matrix. The Unitary matrix is found by performing a singular value decomposition (SVD) onto the previously corrected Jones Matrices as

$$J_{Corrected}^{-1} = L\Sigma R^T$$

from which the Unitary matrix U used is found as

$$U = LR^T$$

Starting from the Unitary matrices calculated at this previous step and by recalling equation 32 it is possible to find the Rotation Muller matrix by letting propagate the horizontal, diagonal and circular polarization (corresponding to the three axes s_1, s_2 and s_3 in Stokes space) through the Unitary matrices[34].

---

[34] Due to the complexity of the operations involved with the calculation of the Rotation Muller Matrix the Unitary matrices have been averaged over windows of 16 non-overlapping values to lighten the computational load.

From the calculated Rotation Muller matrix R the Rotation Vector ϕ is extracted from

$$R = e^{\phi \times}$$

Once the Rotation vectors have been calculated its mean value ϕ_{av} is computed from which the average Rotation Muller matrix is extracted by using equation 46; by using the average Rotation Muller matrix it is possible to compensate the Rotation Muller matrices as

$$R_{compensated} = R_{av}^{-1}R$$

By performing such compensation the rotation vector extracted from the compensated Rotation muller matrix will only be sensitive to the variations with respect to its mean value ϕ_{av}[35].
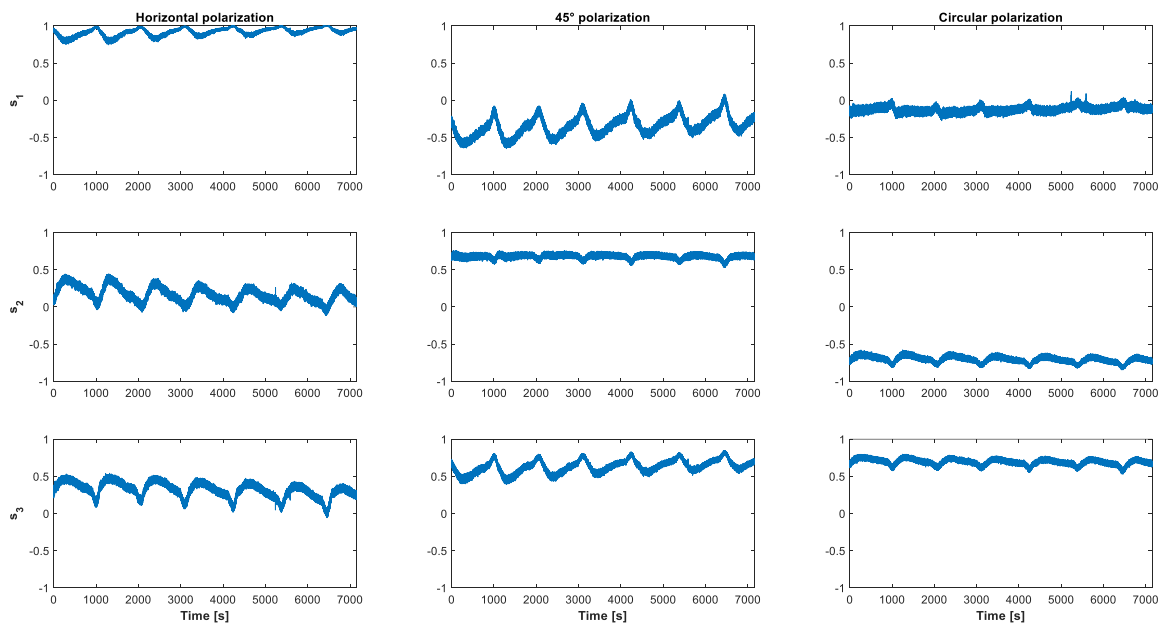

Figure 29 - compensated rotation Muller matrices for a portion of the data

Figure 30 illustrates the spectra (in semi-logarithmic scale) and the related spectrograms for the three components of the rotation vector obtained from the compensated rotation Muller matrices; in the plotted spectres and spectrograms it is possible to see the 3.72Hz frequency and its first harmonics and the 29.79Hz frequency with a trace of its second harmonic that can be seen on the rightmost side of the spectrums.

---

[35] The rotation vector can also be calculated in an easier manner by using $\phi_n = trace\left[\frac{\sigma_n \log{(U)}}{j}\right]$ with n=1,2,3 and with σ_n being the Pauli matrices; while this method is faster the compensation performed by subtracting the mean rotation vector value yields worse results when compared to the method using the Rotation Muller matrices.
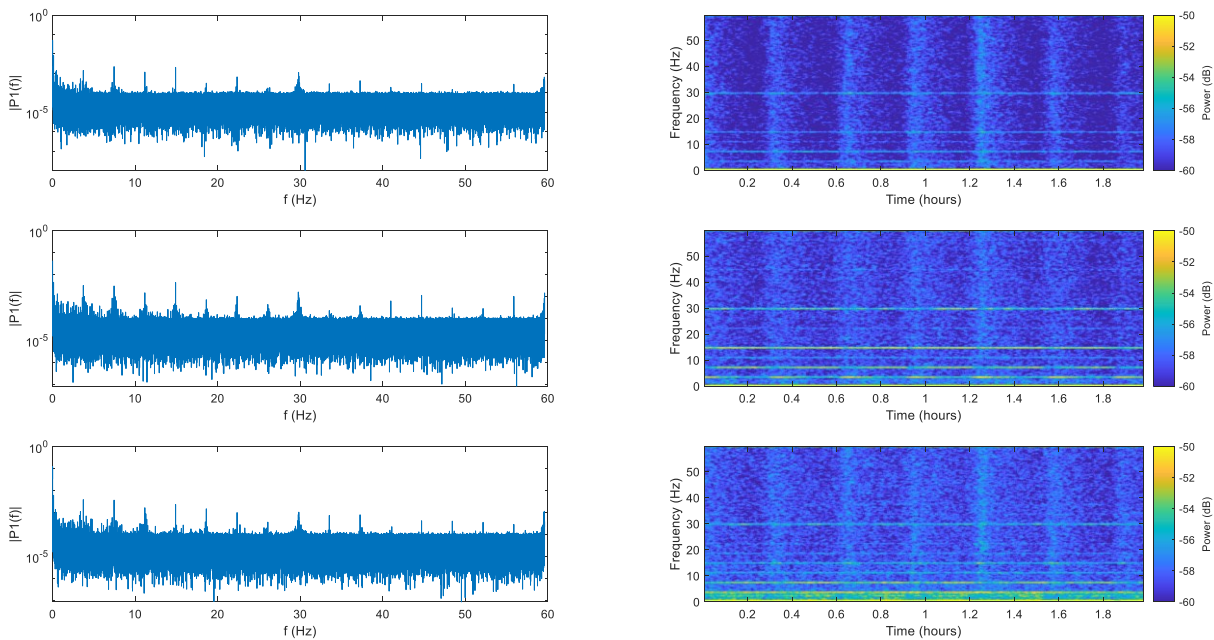
Figure 30 - Spectra and spectrograms of the three components of the rotation vector

While with the performed analysis no peculiar external perturbation was found[36] the most interesting result from this analysis is the ~19min period that can be seen during the whole observation period. This periodicity is probably due to the air-conditioning employed within the lab as 0.66 km of the fibre is located within the laboratory without the outer jacket [31] and so, when compared to the other 5.63 km, it is more sensitive to both temperature changes and the acoustic noise from the fans; this is confirmed by Mazur et al [32] that performed measurements on the same cable that is currently under study reporting among the phenomena that negatively impacted their experiment "*[…] the ventilation system, which turned on/off approximately every 20 minutes to maintain a temperature within 1.5 degC* ".

Another interesting aspect is the 3.72Hz and its harmonics that are present on all the spectrums, this is probably due to the DSP control loop but it can't be confirmed without knowing the full specifics of the DSP system used to acquire the analysed data.

---

[36] During the observation period according to the National Institute of Geophysics and Volcanology (INGV) no major seism took place with the strongest earthquake being a M_L 2.3 at ~16km from the city centre of L'Aquila at a depth of ~15km, probably too weak and far away from the used fibre to be perceived.

CONCLUSION

In this thesis work the equalisation data of a fibre channel has been analysed with the purpose of detecting external events mainly via the observation of the evolution of the state of polarization at the output of the system. Although no particular geophysical event was detected during the observation period the system proved to be able to detect perturbations in the environment such as the ventilation system employed into the lab.

The analysed system in the future, along with the other examples provided in chapter 2, will surely be widely used for seismic sensing using the already existing fibre telecommunication network: this methods in fact have been proven to be reliable and sensitive to even small perturbations like the ventilation system as in chapter 3. These systems can be implemented with little to no cost as they do not require to transmit any signal into the fibre (for polarization-based sensing) or require only with the allocation of a specific wavelength (for phase transmission sensing) and do not need high computational power to perform real-time analysis of the data (all the analysis presented in this thesis work were performed with MATLAB on a laptop computer with calculation times always considerably shorter with respect to the data acquisition period).

By applying these systems to the existing fibre-optic network there would be, as it can be seen in figure 4 and figure 5, a large increase in data coverage for large portions of the seafloor that would help both the field of geophysical research and to create a sturdier earthquake and tsunami warning system.

BIBLIOGRAPHY

[1] R. S. Kerdock and D. H. Wolaver, "Atlanta fiber system experiment: results of the atlanta experiment," *The Bell System Technical Journal,* vol. 57, pp. 1857-1879, 1978.

[2] P. J. Winzer, D. T. Neilson and A. R. Chraplyvy, "Fiber-optic transmission and networking: the previous 20 and the next 20 years [Invited]," *Opt. Express,* vol. 26, p. 24190–24239, September 2018.

[3] I. Roudas, "Coherent Optical Communication Systems," in *WDM Systems and Networks: Modeling, Simulation, Design and Engineering*, N. (. Antoniades, G. Ellinas and I. Roudas, Eds., New, York: Springer New York, 2012, p. 373–417.

[4] E. Ip, A. P. T. Lau, D. J. F. Barros and J. M. Kahn, "Coherent detection in optical fiber systems," *Opt. Express,* vol. 16, p. 753–791, January 2008.

[5] K. Kikuchi, "Fundamentals of Coherent Optical Fiber Communications," *J. Lightwave Technol.,* vol. 34, p. 157–179, January 2016.

[6] K. Kikuchi, "Digital coherent optical communication systems: Fundamentals and future prospects," *IEICE Electronics Express,* vol. 8, p. 1642–1662, 2011.

[7] B. Culshaw and A. Kersey, "Fiber-Optic Sensing: A Historical Perspective," *Lightwave Technology, Journal of,* vol. 26, pp. 1064-1078, June 2008.

[8] B. Lee, "Review of the present status of optical fiber sensors," *Optical Fiber Technology,* vol. 9, pp. 57-79, 2003.

[9] J. Castrellon-Uribe, "Optical Fiber Sensors: An Overview," in *Fiber Optic Sensors*, M. Yasin, S. W. Harun and H. Arof, Eds., Rijeka, IntechOpen, 2012.

[10] A. D. Kersey, "A Review of Recent Developments in Fiber Optic Sensor Technology," *Optical Fiber Technology,* vol. 2, pp. 291-317, 1996.

[11] H. J. W. Strutt, "XV. On the light from the sky, its polarization and colour," *The London, Edinburgh, and Dublin Philosophical Magazine and Journal of Science,* vol. 41, pp. 107-120, 1871.

[12] D. J. Lockwood, "Rayleigh and Mie Scattering," in *Encyclopedia of Color Science and Technology*, M. R. Luo, Ed., New, York: Springer New York, 2016, p. 1097–1107.

[13] M. Cantono, J. C. Castellanos, V. Kamalov, A. Mecozzi, R. Muller, S. Yin and Z. Zhan, "Seismic Sensing in Submarine Fiber Cables," in *2021 European Conference on Optical Communication (ECOC)*, 2021.

[14] M. R. Fernández-Ruiz, M. A. Soto, E. F. Williams, S. Martin-Lopez, Z. Zhan, M. Gonzalez-Herraez and H. F. Martins, "Distributed acoustic sensing for seismic activity monitoring," *APL Photonics,* vol. 5, p. 030901, 2020.

[15] Z. Zhan, "Distributed acoustic sensing turns fiber-optic cables into sensitive seismic antennas," *Seismological Research Letters,* vol. 91, p. 1–15, 2020.

[16] H. Gabai and A. Eyal, "On the sensitivity of distributed acoustic sensing," *Opt. Lett.,* vol. 41, p. 5648–5651, December 2016.

[17] J. Pastor-Graells, H. F. Martins, A. Garcia-Ruiz, S. Martin-Lopez and M. Gonzalez-Herraez, "Single-shot distributed temperature and strain tracking using direct detection phase-sensitive OTDR with chirped pulses," *Opt. Express,* vol. 24, p. 13121–13133, June 2016.

[18] M. R. Fernández-Ruiz, H. F. Martins, E. F. Williams, C. Becerril, R. Magalhães, L. Costa, S. Martin-Lopez, Z. Jia, Z. Zhan and M. González-Herráez, "Seismic Monitoring With Distributed Acoustic Sensing From the Near-Surface to the Deep Oceans," *Journal of Lightwave Technology,* vol. 40, pp. 1453-1463, 2022.

[19] C. Yu, Z. Zhan, N. J. Lindsey, J. B. Ajo-Franklin and M. Robertson, "The potential of DAS in teleseismic studies: Insights from the Goldstone experiment," *Geophysical Research Letters,* vol. 46, p. 1320–1328, 2019.

[20] G. Marra, C. Clivati, R. Luckett, A. Tampellini, J. Kronjäger, L. Wright, A. Mura, F. Levi, S. Robinson, A. Xuereb, B. Baptie and D. Calonico, "Ultrastable laser interferometry for earthquake detection with terrestrial and submarine cables," *Science,* vol. 361, pp. 486-490, 2018.

[21] A. Bogris, C. Simos, I. Simos, T. Nikas, N. S. Melis, K. Lentas, C. Mesaritakis, I. Chochliouros and C. Lessi, *Microwave frequency dissemination systems as sensitive and low-cost interferometers for earthquake detection on commercially deployed fiber cables,* arXiv, 2021.

[22] A. Fichtner, A. Bogris, T. Nikas, D. Bowden, K. Lentas, N. S. Melis, C. Simos, I. Simos and K. Smolinski, "Theory of phase transmission fibre-optic deformation sensing," *Geophysical Journal International,* vol. 231, pp. 1031-1039, June 2022.

[23] D. C. Bowden, A. Fichtner, T. Nikas, A. Bogris, C. Simos, K. Smolinski, M. Koroni, K. Lentas, I. Simos and N. S. Melis, "Linking distributed and integrated fiber-optic sensing," *arXiv preprint arXiv:2205.11065,* 2022.

[24] A. Bogris, T. Nikas, C. Simos, I. Simos, K. Lentas, N. S. Melis, A. Fichtner, D. Bowden, K. Smolinski, C. Mesaritakis and I. Chochliouros, "Sensitive seismic sensors based on microwave frequency fiber interferometry in commercially deployed cables," *Scientific Reports,* vol. 12, p. 14000, 2022.

[25] A. Mecozzi, M. Cantono, J. C. Castellanos, V. Kamalov, R. Muller and Z. Zhan, "Polarization sensing using submarine optical cables," *Optica,* vol. 8, p. 788–795, June 2021.

[26] G. G. Stokes, "On the Composition and Resolution of Streams of Polarized Light from different Sources," in *Mathematical and Physical Papers*, vol. 3, Cambridge University Press, 2009, p. 233–258.

[27] J. P. Gordon, "Statistical properties of polarization mode dispersion," *Journal of Optical and Fiber Communications Reports,* vol. 1, p. 210–217, 2004.

[28] Z. Zhan, M. Cantono, V. Kamalov, A. Mecozzi, R. Müller, S. Yin and J. C. Castellanos, "Optical polarization–based seismic and water wave sensing on transoceanic cables," *Science,* vol. 371, p. 931–936, 2021.

[29] T. Hayashi, T. Sakamoto, Y. Yamada, R. Ryf, R. Essiambre, Jean, N. Fontaine, M. Mazur, H. Chen and T. Hasegawa, "Randomly-Coupled Multi-Core Fiber Technology," *Proceedings of the IEEE,* pp. 1-18, 2022.

[30] C. Xia, N. Bai, I. Ozdur, X. Zhou and G. Li, "Supermodes for optical transmission," *Opt. Express,* vol. 19, p. 16653–16664, August 2011.

[31] T. Hayashi, T. Nagashima, T. Nakanishi, T. Morishima, R. Kawawada, A. Mecozzi and C. Antonelli, "Field-Deployed Multi-Core Fiber Testbed," in *2019 24th OptoElectronics and Communications Conference (OECC) and 2019 International Conference on Photonics in Switching and Computing (PSC)*, 2019.

[32] M. Mazur, R. Ryf, N. K. Fontaine, A. Marotta, E. Börjeson, L. Dallachiesa, H. Chen, T. Hayashi, T. Nagashima, T. Nakanishi, T. Morishima, F. Graziosi, L. Palmieri, D. T. Neilson, P. Larsson-Edefors, A. Mecozzi and C. Antonelli, "Real-Time MIMO Transmission over Field-Deployed Coupled-Core Multi-Core Fibers," in *2022 Optical Fiber Communications Conference and Exhibition (OFC)*, 2022.

[33] E. S. Shivaleela and M. Naveenkumar, "Coherent receivers for fiber optic communications," *ISSS Journal of Micro and Smart Systems,* vol. 11, p. 207–216, 2022.

[34] L. Mescia and F. Prudenzano, "Advances on Optical Fiber Sensors," *Fibers,* vol. 2, p. 1–23, 2014.

[35] R. Piazza and V. Degiorgio, "Scattering, Rayleigh," in *Encyclopedia of Condensed Matter Physics*, F. Bassani, G. L. Liedl and P. Wyder, Eds., Oxford, Elsevier, 2005, pp. 234-242.

[36] N. J. Lindsey and E. R. Martin, "Fiber-optic seismology," *Annual Review of Earth and Planetary Sciences,* vol. 49, p. 309–336, 2021.

[37] A. Fichtner, A. Bogris, T. Nikas, D. Bowden, K. Lentas, N. S. Melis, C. Simos, I. Simos and K. Smolinski, "Introduction to phase transmission fibre-optic sensing of seismic waves," *arXiv preprint arXiv:2202.13574,* 2022.

[38] M. Cantono, V. Kamalov, V. Vusirikala, M. Salsi, M. Newland and Z. Zhan, "Sub-Hertz Spectral Analysis of Polarization of Light in a Transcontinental Submarine Cable," in *2020 European Conference on Optical Communications (ECOC)*, 2020.

[39] E. Collett, Field Guide to Polarization, Society of Photo Optical, 2005.

[40] J. P. Gordon and H. Kogelnik, "PMD fundamentals: polarization mode dispersion in optical fibers.," *Proceedings of the National Academy of Sciences of the United States of America,* vol. 97, no. 9, pp. 4541-50, April 2000.

[41] B. Saleh and M. Teich, Fundamentals of Photonics, 2nd Edition, 2007.

[42] D. Bacco, N. Biagi, I. Vagniluca, T. Hayashi, A. Mecozzi, C. Antonelli, L. K. Oxenløwe and A. Zavatta, "Characterization and stability measurement of deployed multicore fibers for quantum applications," *Photon. Res.,* vol. 9, p. 1992–1997, October 2021.

[43] D. J. Richardson, J. M. Fini and L. E. Nelson, "Space-division multiplexing in optical fibres," *Nature Photonics,* vol. 7, p. 354–362, 2013.